# The marginal congestion
# of a taxi in New York City

Daniel Mangrum[*]          Alejandro Molnar[*]
Vanderbilt University      Vanderbilt University

November 12, 2018[†]

## Abstract

We exploit the partial deregulation of New York City taxi medallions to provide a causal estimate of the impact of taxi supply on congestion. We employ taxi trip records to measure historical street-level speed. We find that the roll-out of newly authorized taxis caused a local 8-9% decrease in speed. We estimate an empirical congestion elasticity curve from heterogeneous changes in speed and taxi supply, counted from aerial orthoimagery. Additionally, we provide novel urban sensor data to document a substantial traffic slowdown since 2013. Most of the slowdown in midtown Manhattan is accounted for by new supply from ridehail applications.

Keywords: Urban transportation. Congestion. Externalities. Regulation. Taxi. Rideshare. Ridehail. Transportation Network Companies. JEL: D22, D62, L91, L92, R41, R42

The congestion of transportation infrastructure has both macro and microeconomic costs. Transportation affects the organization and scale of economic activity in cities (Redding and Turner, 2015; Ahlfeldt *et al.*, 2015): while agglomeration saves transportation costs, these savings diminish as density congests infrastructure. When transportation infrastructure becomes congested, residents both bear and impose external costs. In the context of road congestion, costs include the value of time (Anderson, 2014), pollution and health (Currie and Walker, 2011; Knittel *et al.*, 2016), carbon emissions (Barth and Boriboonsomsin, 2008) and subjective well-being (Kahneman and Krueger, 2006; Anderson *et al.*, 2016).

We document that traffic in New York City, one of the most productive cities in the United States (Hsieh and Moretti, 2017), has slowed down substantially since 2013. Taxi trips within midtown Manhattan have slowed down on the order of 15%, but the slowdown is widespread: it shows up in taxi trip records throughout the day and over the entire city, on highways – as measured though a novel dataset that we assemble from EZ-pass sensors – and in responses to the American Community Survey.

Cities such as New York are undergoing technological and policy changes with uncertain costs and benefits: roads may be under increasing demand from transportation network companies (also known as ridehail) and parcel delivery services, while space in the city is increasingly allocated to bikeshare, bike lanes and pedestrians (Sadik-Khan and Solomonow, 2016).

We evaluate a policy change that is unique to New York City: starting in August 2013, the city partially deregulated its medallion taxi industry by authorizing a new class of taxi. "Boro" taxis are almost identical to the city's 13,237 traditional yellow medallion taxis, but are painted green and are restricted from picking up passengers at airports or in Manhattan south of East 96th street and West 110th Street. We exploit the unique natural experiment provided by the roll-out of up to 6,539 new taxis searching for passengers under a well-defined spatial constraint to causally estimate the impact of taxi supply on traffic congestion in New York City.

We employ a dataset with 1.3 billion taxi trip records from 2009 to June 2016, which contain precise times and geographic coordinates of pickups and dropoffs, to construct a dataset of street-level speed that spans both sides of the exclusion boundary in northern Manhattan and the period prior to and after the roll-out of boro taxis. Our measures of speed are constructed at a high spatial resolution by selecting the trips that involved a pickup and a dropoff along the same avenue (about 69,300 trips per month in our area of interest) and either averaging or projecting travel times onto street segments or flexible functions.

Avenues flow faster toward the north of Manhattan, as density and traffic decline,

and all avenues have slowed down over time. Following the introduction of boro taxis, however, a stark speed gap opened up north of the boro taxi exclusion boundary (see Figures 2 and 3). In our baseline estimates we find that the boro program's roll-out caused an overall 8-9% slowdown in the speed of traffic in northern Manhattan.

Our estimates are robust to controlling for observable changes in road use (such as the deployment of bike lanes and bikeshare, among others), as well as a large set of specifications to address unobservable confounders. Unobservables that could be a cause for concern include differential trends over the city's geography (for instance, due to economic recovery or gentrification) or a differential impact from the arrival and growth of ridehail as a transportation alternative. Estimates of the boro program's impact track the timing of the roll-out of taxi supply, which ramped up over the last quarter of 2013, and are identified under narrow time windows around the roll-out. Our estimates are also robust to trends by avenue and treatment status that are linear in time but are also allowed to kink and track the rapid growth in ridehail. We also find that our results are not sensitive to differential time trends over space in the measurement error of geographic coordinates, a potential confounder in research that employs data from GPS units within dense urban settings. We address spatial spillovers, which could arise naturally as boro taxis transport passengers south of the pickup exclusion boundary, and congestion could be transmitted across the boundary through gridlock: alternative estimation strategies (which include a triple-difference interaction that exploits the direction of traffic, as well as spatial econometric models allowing for links between street segments) are consistent with the upper range (9%) of our impact estimates.

We next quantify the impact of boro taxis not in terms of the deregulation episode as a whole, but in terms of taxi supply. As a benchmark, we employ the taxi trip data to measure taxi activity in pickups and instrument for pickups with the boro taxi roll-out; we then rescale a congestion elasticity estimated in terms of pickup units to supply using a back-of-the-envelope proportionality assumption. Recent research on the taxi industry, however, has emphasized that pickups are the observed equilibrium outcome of search between unobserved demand and supply (Buchholz, 2017; Frechette *et al.*, 2016).[1] In our context, this implies that taxi pickups and supply may not be in proportion to each other.

We address the observability of taxi supply by collecting a sample of 29 aerial orthoimagery scenes going back to 2010. We digitize the location of 132 thousand

---

[1] See also Lagos (2003) for an earlier analysis using a survey of taxi trip sheets (an earlier generation of taxi trip record data, hand-recorded by drivers with coarse location identifiers). The taxi record data we employ has been used to study labor supply (Farber, 2015), moral hazard in contracting (Schneider, 2010; Jackson and Schneider, 2011), behavioral cues (Haggag and Paci, 2014) and learning (Haggag *et al.*, 2017), but not to estimate congestion externalities in transportation.

yellow taxis, boro taxis and other vehicles in the imagery. Our data allows us to measure changes to the patterns of vehicle density over space, comparing the period before and after the roll-out of boro taxis.[2] Our data can be used to estimate the relationship between supply and taxi matches. We use it to directly measure changes in taxi supply at a high degree of spatial resolution, which we relate to a set of heterogeneous speed impacts estimated over the boro taxi zone. Heterogeneity in impacts is related to baseline traffic density. We obtain a distribution for the ratios of changes in travel time to changes in supply, i.e. congestion elasticities. We plot our measured elasticities against baseline taxi density to non-parametrically estimate a marginal congestion curve that is identified from the supply shock produced in northern Manhattan by the boro taxi program. We find that congestion elasticity from taxi supply rises and is slightly convex in density, reaching 0.30 at the higher range that best extrapolates to denser areas in midtown Manhattan.

Lastly, we apply our estimated congestion elasticity curve with a study of New York City's slowdown since 2013. We document the slowdown using taxi meter data and by contributing two new sets of time series to the state of knowledge on traffic speed and volumes in New York City: i) archived highway speeds reported from a network of EZ-pass sensors, and ii) vehicle miles traveled by vehicle class, estimated from odometer inspections. New York City policy makers have failed to find a link between growth in the supply of ridehail and the city's slowdown. As we discuss below, the city's congestion studies do not employ the available data exhaustively and fail to meet the standards of modern empirical research.

We digitize aerial imagery samples in an area of midtown Manhattan and find a 14.1% increase in vehicle density since the summer of 2013 over the prior three years. We also detect a substantial change in the observed color composition of (non-taxi, non-truck) cars in midtown Manhattan: whereas 29.3% of cars counted in overhead imagery prior to the summer of 2013 were black, that share has since increased to 45.7%. VIN-level records from the New York state Department of Motor Vehicles indicate that while 20.9% of privately owned cars in New York City are black, 73.0% of For-hire vehicles (FHVs, a category that includes ridehail) are black. Employing color-share data, we estimate that the density of for-hire vehicles in midtown Manhattan has increased by

---

[2] To our knowledge, ours is the first application of vehicle counts from aerial imagery in economics, or to the study of the long-run impact of regulation on vehicle density and congestion in any discipline. See Donaldson and Storeygard (2016) for a discussion of satellite imagery in economics. Traffic engineers have employed aerial imagery for decades (e.g. Johnson, 1928; Greenshields, 1948) for infrastructure design studies and more recently to calibrate agent-based models of traffic flow. A recent literature in machine learning addresses the detection of vehicles from aerial images (e.g., Reilly *et al.*, 2010, Mundhenk *et al.*, 2016; Razakarivony and Jurie, 2016) but its output has yet to be applied in empirical research.

222.9% since the summer of 2013. We also estimate a 6.8% decline in the number of private cars on the road.[3] Taking a 15.2% median slowdown in midtown Manhattan and a 0.30 estimated congestion elasticity as reference values, we find that the 30.5% increase in the joint supply of taxis and FHVs in midtown Manhattan over the past three years (taxis down 11.8%, FHVs up 222.9%) can account for 61.8% of the slowdown in traffic. Overall, evidence from aerial counts and the spatial and time series patterns of New York City's slowdown do not appear to be consistent with rival explanations such as bike lanes, construction or use by cyclists, pedestrians or trucks.

Section 1 below describes the boro taxi program. In Section 2 we use taxi trip records to build historical street speed data. In Section 3 we estimate the impact of the boro program on traffic speed. In Section 4 we derive a congestion elasticity curve for New York City in terms of taxi supply. In Section 5 we apply our estimated congestion curve to the issue of increased vehicle density due to supply growth from ridehail. Section 6 concludes.

# 1   Taxi regulation in New York City and the launch of "boro" taxis

Taxi service in New York City is regulated by the Taxi and Limousine Commission (TLC). Among other regulations, the TLC sets fares, licenses drivers and cars and issues medallions, which are a fixed number of permits that must be attached to a licensed car for it to operate as a taxi (i.e. accept street hails) in the five boroughs of New York City. The number of medallions was fixed at 11,787 for decades, with a few small increases after 1996, and remained at 13,237 between May 2008 and August 2013. The only type of medallion taxi available up to August 2013 was the traditional yellow taxi. Although yellow taxis are statutorily allowed to pick up passengers in all five boroughs of New York City, most taxi pickups occurred in Manhattan, particularly midtown, and at the city's two airports. The spatial distribution of yellow taxi pickups is illustrated in Figure F.6 using data for June 2013. Areas outside of northern Manhattan and the remaining four boroughs had limited taxi coverage, and throughout most of New York City residents could not dependably hail a yellow taxi from the curb. Prior to ridehail apps the most common method for residents in the outer boroughs to hire

---

[3] Aerial images combined with color-share data allow us to separately estimate the density of vehicles other than taxis, such as private cars and ridehail. An advantage of our approach is that we can measure vehicle density in dense, downtown city streets. Previous studies using counts from loop detectors, stationary traffic cameras or gantries (e.g. Xie and Olszewski, 2011; Li *et al.*, 2017) are usually limited to highways or arterial roads.

car transportation was to call radio-dispatch bases for pre-arranged transportation from "for-hire vehicles," as well as unlicensed street-hails offered by some for-hire vehicles and other informal providers.[4]

In August 2013 a new class of taxi was allowed on the road: painted green and referred to in regulation as "street-hail livery" (SHL) taxis, or alternatively as "boro" or green taxis, these taxis and their drivers are regulated like yellow taxis with a major distinction: passenger pickups (whether pre-arranged or street-hails) are not allowed at the two city airports or south of East 96th Street and West 110th Street in Manhattan, an area referred to as the "hail-exclusion zone." The objective of the boro taxi program was to increase street-hail availability in the outer boroughs and provide a regulated alternative to unlicensed street-hails.[5] Following a multi-year political and regulatory process, the roll-out of the boro program involved an initial sale of 6,000 medallion permits, as well as a fleet roll-out and driver recruitment process carried out by medallion owners. Additional permits were put on sale in August 2014. Figure 4 contains a timeline of the number of unique boro taxis that recorded at least one trip during each month.

## 2    Reconstruction of historical street speeds from taxi trip data

There is no publicly available dataset that contains information on street speed at a high level of spatial resolution in New York City and over a historical period going back prior to the roll-out of the boro taxi program.[6] In this section we describe how we employ historical records of taxi trips from the Taxi and Limousine Commission (collected from GPS-enabled taxi meters since 2009 under the "Taxicab Passenger Enhancement Program") to construct measures of historical street speeds, using three alternative methodologies. In the next section we employ these measures as outcome variables to quantify the impact of the roll-out of the boro program over space and time.

---

[4] See Gao Hodges (2012) for the history of the city's taxi cab industry, including unlicensed activity.

[5] See www1.nyc.gov/office-of-the-mayor/news/362-13/mayor-bloomberg-more-1-000-boro-taxis-now-new-york-city-street for a NYC government press release on the roll-out of the program and its intended goals. Other differences with yellow taxis are that 20% of boro medallions require the taxi to be wheelchair-accessible, and the taxis are required to undergo vehicle inspections at half the regularity of yellow taxis.

[6] Recent studies of traffic congestion have employed probe data from cell-phones, obtained from the Google maps API (e.g. Hanna *et al.*, 2017; Akbar and Duranton, 2017), but historical data was not available to us over our period of study. Additionally, travel time APIs are developed with the aim of prediction and their methodologies may changed in ways that render them not comparable over long periods or over space. Another alternative, the INRIX dataset, is constructed from probes on fleets of commercial vehicles and is not as attractive as our methodology for dense urban settings such as New York City.

## 2.1 Average travel times at a 10 meter resolution

The simplest approach to measuring the speed of traffic, and the approach we favor throughout the paper, is to average the rate of travel across all taxi trips for which we are confident that the taxi traversed a certain interval over a certain period. To estimate average travel times at a specific time and place, for each month in the data we select the taxi trips that were entirely contained within a rectangular strip running along one of the north-to-south avenues of Manhattan, and in which the pickup and drop-off locations are oriented in the direction of traffic. On avenues with two directions of traffic, such as Park Avenue, we classify trips according to direction. We refer to each avenue and direction of traffic as a "run."

Every trip record contains the time as well as the latitude and longitude for each pickup and drop-off, as provided by a GPS-enabled taxi meter. We project the coordinate of each endpoint perpendicularly onto a straight line down the center of each avenue, allowing us to locate each trip endpoint on this line. We then calculate for each trip the ratio of the travel time to the line distance, to obtain each trip's average seconds per meter (i.e. the inverse of speed). To calculate average seconds per meter at a 10 meter resolution, we subdivide each run into 10 meter intervals (or "bins"), and for each of these average the travel time per meter of all the taxi trips that fully traversed the interval. Variation in the average travel time between bin $i$ and bin $i+1$ therefore comes from the variation in the average travel times of taxi trips that fully traverse bin $i$ but not bin $i+1$, or vice-versa.[7]

Since our objects of interest are (averages of) speed over a particular segments, the averages obtained by the method described above could be subject to biases due to aggregation as well as changes in trip selection over space and time. As an example of this potential concern, consider two 10 meter bins in a relatively uncongested area in the north of the city, and assume traffic moves at the same speed along both bins. Suppose the northernmost of these bins contains a hotel driveway, whereas its neighbor to the south does not. The bin containing the hotel originates many long trips to a congested downtown area, whereas the neighboring bin originates short trips within a relatively uncongested interval. In this example, the average taken over the travel time of the trips crossing each bin will be upwardly biased as an estimator of the true marginal travel time of crossing each bin due to congestion that affects the taxis traveling downtown from the hotel (an aggregation bias) and, further, the bias will be larger for the bin containing the hotel since its average does not contain the short, local trips originating

---

[7] The within-avenue sample is presented in Table 2. The outcome of the data construction step is plotted in Figures 2 and 3. For ease of presentation, it is averaged again at the annual level, and expressed in miles per hour, rather than seconds per meter. Observable changes in speed are discussed in Section 3 below.

in the southern neighbor (a selection bias). Aggregation bias can also interact with time, as the bin may be located next to a nightclub or park, and trips may originate at times when traffic is lower, such as nights or weekends.

A third type of potential bias could arise from the type and behavior of the "probe" that provides a taxi trip record, e.g. whether a car is a yellow or boro taxi. We employ data on both types of taxis, since boro taxis increase the sample in the north of the city, but for this reason and because boro taxi trips are by definition only possible after the launch of the boro program, variation across taxi type in driving speed would bias our travel time estimates in a manner that could violate parallel-trend assumptions required for difference-in-differences evaluation. To investigate this possibility, we exploit the fact that the data contains approximately half a million trips per day to isolate quasi-experimental "taxi race" conditions in which both a yellow and a boro taxi both picked up and dropped off a passenger within 10 meters of each other, as well as within a minute of each other. We find 234 such natural experiments in our area of northern Manhattan. We then regress travel time outcomes on a fixed effect per "taxi race" and a binary indicator for the boro taxi in the pair. Results are reported in Table 1. We find positive but non-significant coefficients in travel time levels, logs or ratios (i.e. seconds-per-meter). Since the magnitude of the estimated coefficient is a non-trivial 2.5% speed difference, we explore relaxing the threshold on pickup time difference from one minute apart to two, and up to 12, and find results that are statistically significant at the 5% level in a couple specifications in logs, as well as in levels, although not in seconds-per-meter. Alternative specifications intended to control for within-experiment variation in observables (such as a "pole position" effect, number of passengers or the residual variation in trip distance on the taxi meter) do not affect the results. We take this collectively as evidence that there may be a small difference in driving speeds for boro and yellow taxis.[8]

We develop two alternative estimates of travel time to address the issues discussed in this section, but before developing these we discuss a brief pre-existing literature: to our knowledge, no previous paper has recovered street speeds from taxi GPS "probe" data in a manner that resolves the aggregation issues described above, or employed such estimates for the evaluation of urban transportation policy. Three prior papers in the computer science literature, however, have developed methods to reconstruct street speeds for the purposes of exploratory and descriptive analysis within a large urban

---

[8] A reason for this speed difference could be that a higher proportion of boro taxis are wheelchair-accessible vans, and these vehicles may accelerate more slowly than the average taxi. Alternatively, since daily rental rates (for medallion and car) are lower for boro than yellow taxis, it may be the case that drivers respond to the different opportunity costs of time, or that the activity of driving a boro taxi selects drivers with a lower subjective opportunity cost of time, i.e. slower drivers.

area. Zhan *et al.* (2013), Santi *et al.* (2014) and Poco *et al.* (2015) are concerned with recovering speeds on street segments from the TLC trip data given that trip origins and destinations are located on the NYC road network and the path taken by the driver is unknown. The approach taken in these papers is to employ a routing algorithm to determine a set of latent, unobserved paths, and then allocate total trip travel times to weighted segments from the latent paths. Since our focus is precision within a specific area of interest, rather than exploratory analysis, we circumvent the path attribution problem by employing only the subset of trips whose origin and destination are located along the same avenue and in the direction of traffic. Conditional on a given latent path, Santi *et al.* (2014) and Poco *et al.* (2015) average travel times over trips crossing a segment and are therefore identical to our approach in this section, whereas Zhan *et al.* (2013) project trip times onto segment dummies and are therefore identical to the approach we describe in the next section, although their approach does not contain controls for observable trip characteristics, (e.g. driver type, or distance from GPS coordinates to grid network), or allow for non-linearity arising from fixed and variable components of travel time cost (e.g. due to acceleration).

## 2.2 Projection on dummies to recover a travel time function

Our first approach to estimating marginal travel times at the street level while controlling for spatial and temporal aggregation bias consists of projecting travel times onto dummy variables for the intervals that are traversed by each individual trip, as well as observables such as taxi type. This approach is intended as an intermediate illustration for our next approach, so we present it in a summary manner.

We predefine a set of interval bins $b = \{\underline{b}, \ldots, \bar{b}\}$ of varying width over several city blocks, and construct a set of indicators variables $m_{bi}$ that are turned off at a value of zero if a taxi trip does not intersect the interval and are turned on at a value equivalent to the width of an interval if the trip intersects it (this is equivalent to regressing travel time on dummies and appropriately rescaling coefficients after estimation). We also define sets of binary indicators that turn on if trip $i$ starts ($s_{bi}$) or ends ($e_{bi}$) in a given interval. For each month and uptown or downtown "run" along an avenue, we project the travel time $T_i$ of trip $i$ onto these indicators:

$$T_i = \sum_{b=\underline{b}}^{\bar{b}} \beta_{mb} m_{bi} + \sum_{b=\underline{b}+1}^{\bar{b}-1} \beta_{sb} s_{bi} + \sum_{b=\underline{b}}^{\bar{b}} \beta_{eb} e_{bi} + \beta x_i + \delta_h + \varepsilon_i \tag{1}$$

where additional controls include hour fixed effects, two alternative controls for boro

taxi status (a dummy, consistent for a fixed cost, and a trip distance measure interacted with boro taxi status, consistent for a boro variable cost) and a control for "surplus distance" on the taxi meter after the coordinates of each trip endpoint undergo a perpendicular projection onto the straight north-south line along each avenue. Each trip will also turn on an indicator dummy both for both endpoints, as well as a number of middle indicators. Because we observe trips that fully traverse the intervals $b = \{\underline{b}+1, \ldots, \bar{b}-1\}$, and have saturated the specification with terms that can absorb contributions to travel time from trip events other than the crossing of these intervals, the estimated coefficients $\hat{\beta}_{mb}$ for $b = \{\underline{b}+1, \ldots, \bar{b}-1\}$ are consistent for (an average over) the interval marginal second per meter function specific to bin $b$, whereas the coefficients on $\hat{\beta}_{mb}$ for $b = \{\underline{b}, \bar{b}\}$ are consistent for an average of the marginal second per meter function over the fractional measures of the interval that are intersected in the data, which are not a quantity of interest and are discarded. All of the coefficients on $\hat{\beta}_{sb}$ and $\hat{\beta}_{eb}$ play a similar role, as they are consistent for average marginal costs on fractionally traversed intervals, and are also discarded. Given that trip data is only observed in the interior of the interval defined by the lower limit of $\underline{b}$ and the upper limit of $\bar{b}$, the average speed parameters $\beta_{mb}$ for $b = \{\underline{b}, \bar{b}\}$ are not identified. The estimated coefficients $\hat{\beta}_{mb}$ for $b = \{\underline{b}+1, \ldots, \bar{b}-1\}$ constitute our second measure of an underlying "seconds-per-meter" travel time function. These estimates control for spatial aggregation bias, since travel times are projected linearly onto the event of crossing specific intervals, and so estimates are computed from differences in the overlaps between intervals traversed. Continuing with the hotel example from above, if variation elsewhere in the data identifies downtown segments as being particularly slow, this high time cost will be subtracted from the southbound trips originating at the hotel, allowing travel time in the hotel's interval to be identified from that interval's actual contribution to travel time (lower, in our example). This method also allows us to include hour fixed effects to control for the time aggregation bias that would arise from correlation between trip endpoints and time of day, as well as controls for trip observables.

The projection on dummies method does have some costs, however, as it involves substituting variance for bias. Discretizing the "second per meter" travel time function into a set of intervals leads to loss of information, as the method discards average travel time data on the portion of each trip that does not fully traverse an interval. Discretization cannot be made arbitrarily low in a finite sample: it will eventually lead to intervals that do not originate or end trips, causing identification failure as the projection matrix loses full rank. Since estimates in the projection method are obtained from differencing time costs across intervals, errors in one interval can propagate to

10

others, leading to high variance of estimates. The discontinuity in the seconds-per-meter function that is imposed as an assumption on the data generating process is one source of variance, as it leads to abrupt changes in the travel times that are attributed to otherwise similar trips if only one of these crosses the junction point used in discretization.[9] To address these concerns, our next method also controls for potential aggregation bias while delivering a better trade-off in terms of reduced variance.

## 2.3  Projection on B-splines to recover a travel time function

Our second projection method controls for aggregation bias and observable trip characteristics in the same way as the projection dummy method above, but explicitly models a continuous "seconds per meter" function with basis splines: the advantages of this method are that it eliminates discontinuities at junction points between interval dummies, and that it eliminates data loss on trip segments that do not fully traverse a discrete interval, both of which reduce the variance of estimates. Additionally, this method produces a flexible estimate for the "seconds per meter" function that can be evaluated at every point of its support.

Let $s$ be the true "seconds per meter" function, which is defined over an interval of road during a given month. A taxi trip $i$ that begins at point $a_i$ and ends at point $b_i$ on the interval will take a total time:

$$T_i = \beta_1 x_{1i} + \int_{a_i}^{b_i} [s(\tau) + \beta_2 x_{2i}] d\tau + \varepsilon_i \tag{2a}$$

$$T_i = \beta_1 x_{1i} + S(b_i) - S(a_i) + \beta_2 (b_i - a_i) x_{2i} + \varepsilon_i \tag{2b}$$

where $x_{1i}$ are trip characteristics that do not depend on location or trip distance (i.e. fixed time costs), $x_{2i}$ are trip characteristics that depend on trip distance but not location (variable time costs) and $S(b_i) - S(a_i)$ is the area under the seconds-per-meter function. We can estimate (Eq. 2b) by regressing $T_i$ on the spline differences $[S(b_i) - S(a_i)]$, $x_{1i}$ and $(b_i - a_i) x_{2i}$, which we can implement using basis splines for the location of trip origins and destinations, provided we impose the constraint that the spline function is the same at both endpoints.[10]

---

[9] In our application, we employ as few at seven intervals and obtain estimated travel times that are *negative* in 1.7% of all run-bin-month cells.

[10] Our specification for the error term assumes that it is additive to integrated travel time. Alternatively, we could assume an instantaneous mean zero error that arises over the interval. In this case we would have that $T_i = x_{1i} + \int_{a_i}^{b_i} s(\tau) + \beta x_{2i} + \varepsilon_i(\tau) d\tau$ and so we could write $T_i = x_{1i} + S(b_i) - S(a_i) + \beta (b_i - a_i) x_{2i} + (b_i - a_i) \bar{\varepsilon}_i$ where $\bar{\varepsilon}_i = (b_i - a_i)^{-1} \int_{a_i}^{b_i} \varepsilon_i(\tau) d\tau$ is a heteroskedastic error term. We could estimate this

To implement B-splines, if we let:

$$S(\tau) = \sum_{k=1}^{K} \gamma_k \psi_k(\tau)$$

where $\psi_k$ are the bases of the spline, then the regression above can be written as:

$$T_i = \beta_1 x_{1i} + \sum_{k=1}^{K} \gamma_k \left[\psi_k(b_i) - \psi_k(a_i)\right] + \beta_2 (b_i - a_i) x_{2i} + \varepsilon_i \tag{3}$$

which can be estimated by OLS. Since the bases $\psi_k(\tau)$ are differentiable, after estimation we can recover

$$\hat{s}(\tau) = \hat{S}'(\tau) = \sum_{k=1}^{K} \hat{\gamma}_k \psi'_k(\tau)$$

where $\hat{\gamma}_k$ are coefficients estimated by OLS.

# 3 Impact of the boro program on traffic congestion

Historical data on street speed at a high level of spatial resolution allows us to evaluate the impact of policies that impact road use in a well-defined spatial manner. In this section we describe how we exploit the roll-out of the Street-Hail Livery program to evaluate the impact of boro taxis on congestion in northern Manhattan. Our area of study spans 1 kilometer of the Upper East Side and 2 km of East Harlem on the East Side, and 2 km of Upper West Side and 1 km of Morningside Heights and Harlem on the West Side. Urban density and socioeconomic status decline towards the north, although not in a monotone or smooth manner. Prior to the launch of the boro program, the declining gradient in urban density was associated with lower yellow taxi pickup activity, with spikes around major intersections, which include subway stations.[11] The boro taxi program was intended to increase supply in areas undeserved by traditional

---

equation by GLS, or divide both sides by $(b_i - a_i)$:

$$\bar{s}_i = \frac{T_i}{(b_i - a_i)} = \beta_1 \frac{x_{1i}}{(b_i - a_i)} + \frac{S(b_i) - S(a_i)}{(b_i - a_i)} + \beta_2 x_{2i} + \bar{\varepsilon}_i$$

where $\bar{s}_i = \frac{T_i}{(b_i - a_i)}$ is a trip's average seconds per meter. We can then implement a regression of $\bar{s}i$ on rescaled splines differences $\left[\frac{S(b_i) - S(a_i)}{(b_i - a_i)}\right]$ and $x_i$, which imposes the GLS correction for heteroskedasticity under the assumption of integrated errors.

[11] As shown in Fig. F.6 most yellow taxi activity is concentrated at airports as well as midtown and downtown Manhattan.

yellow taxis, but its implementation through a "hail-exclusion" zone south of East 96th and West 110th streets creates an incentive for boro taxi drivers to cruise for hails in the area just north of the boundary: whereas this area was of marginal cruising value for yellow taxi drivers, it is a corner-solution for boro taxi drivers, leading to a localized shock to supply.[12]

Our empirical strategy in this section consists of exploiting this localized shock, and its roll-out over time, to evaluate the impact of boro taxis. Figures 2 and 3 show the average travel time measures (estimated as described in Section 2.1) for all the avenues that contain useful variation to identify the main results in the paper.[13] For ease of presentation the data has been averaged at the annual level, and expressed in miles per hour, rather than seconds per meter. Inspection of these figures reveals the identifying variation in the data and that drives our main difference-in-differences estimates: historical speeds increase in the northern direction along most avenues, along with declining urban density and traffic,[14] and as time goes on all streets become slower, but particularly so north of the hail-exclusion boundary, an area we refer to as "boro-zone." Particularly stark examples include 5th Ave (Fig. 3a) and Lexington Ave (Fig. 3e), but the result can be observed on most avenues.

We employ a difference-in-differences specification to estimate an average reduced-form impact from the boro taxi program on street speed in northern Manhattan. Let $s_{rbm}$ be a travel time outcome, which in most specifications is the log seconds per meter at the level of an avenue run ($r$), 10 meter bin ($b$) and month ($m$) from January 2009 to June 2016. In a standard difference-in-differences specification we would define the post dummy as August 2013 and all months thereafter:

$$s_{rbm} = \beta_{DID}\text{post}_m \times \text{boro zone}_{rb} + \beta x_{rbm} + \text{fixed effects} + \varepsilon_{rbm} \qquad (4)$$

However, the supply of boro taxis was rolled-out gradually: only 114 boro taxis carried out at least one trip during the program's first month of August 2013, and this number rose to 445 taxis in September, 1,128 in October, 1,754 in November and 2,736 in

___

[12] This notion holds under a spatial search equilibrium as in Buchholz (2017): areas with high baseline demand support higher search in equilibrium, although the endogenous continuation value for above-boundary pickups may be shaded down by a higher transition probability into the hail-exclusion zone.

[13] Some avenues, such as West End, Amsterdam downtown or Columbus uptown do not cross the hail-exclusion boundary and therefore do not contain identifying variation after we include fixed effects at the avenue level. We also drop Manhattan Ave since it does not contain sufficient trips north of the boundary to reliably estimate speed.

[14] This is always the case on the East side, but not on the West side where some avenues both narrow and become two-way north of the hail exclusion boundary. The time-invariant attributes of streets, such as changes in width, the direction of traffic, or bends in the roadway will be absorbed in specifications described below by fixed effects at the level of the avenue run and 10 meter bin.

December. Although this ramp-up was relatively fast, it took until June 2015 for the program to reach the highest number of boro taxis ever observed to be active in a given month, which was 6,539. The time series for the number of unique boro taxis is plotted as the solid green line in Figure 4. We define the *boro roll-out$_m$* treatment intensity measure as the ratio of boro taxis active each month (zero prior to August 2013) to the maximum value of 6,539, and our preferred specification is to employ this intensity measure in difference-in-differences specifications of the form:

$$s_{rbm} = \beta_{DID}\text{boro roll-out}_m \times \text{boro zone}_{rb} + \beta x_{rbm} + \text{fixed effects} + \varepsilon_{rbm} \qquad (5)$$

Our baseline specifications include fixed effects $\delta_{rb}$ at the level of each run and bin, absorbing time invariant features of the road, as well as a set of monthly time-effects $\delta_{rm}$ at the level of each run, which absorb the variation in speed along each avenue over time that is common across bins. The main difference-in-differences coefficient under this fixed effect specification is estimated from the differences within each avenue between the travel time north vs. south of the hail-exclusion boundary as the boro program was rolled out. For regressions based on eqs. (4) or (5) to provide an estimate of the causal impact of the boro program we require the parallel trend assumption that street speed in the hail-exclusion "control" zone and boro "treatment" zone are not trending apart from each other for reasons other than the impact of the program. We will discuss below the robustness of our estimates to trends in unobservables, along with alternative fixed-effect structures and specifications, but first we consider a number of observable features of the urban environment that vary at the level of road segments over time and could act as confounders for our estimate of the boro program's impact on traffic speed.

A first source of potential, observable confounders consists of changes in the use of road space, for example for transportation alternatives. Bike lanes were expanded substantially throughout NYC during the period of our study, so we use time-stamped maps of the bike lane network to control for bike lane expansion in our area of study.[15] A second change in transportation infrastructure with a potential impact on road use and traffic speed was the deployment and northward expansion of the Citibike bikeshare system. Citibike launched south of Central Park - outside our area of interest - in May 2013, but expanded into the upper east and west sides over the summer of 2015. We map the deployment of Citibike stations over time as well as, in an alternative specification, all areas along an avenue south of any newly opened Citibike station, to control for both stations and cyclists.[16] Additional potential confounders include changes to road

---

[15] See Sadik-Khan and Solomonow (2016) for the former NYC Department of Transportation commissioner's account of the substantial expansions in bike lanes and pedestrian plazas over this period.

[16] See Molnar and Ratsimbazafy (2016) for a study of the Citibike bikeshare program and its impact on

conditions. We construct count measures at the road-segment level for complaints reported to the city's "311" municipal services hotline, for conditions that could impinge traffic. We also construct count measures for outstanding potholes. Additionally, two re-zoning events took place during our period of study, the establishment in June 2012 of Special Enhanced Commercial Districts 2 and 3 along a number of avenues on the Upper West Side. Although this re-zoning was entirely commercial in character, intended to regulate "ground floor frontages" to preserve commercial activity and "multi-store character," in some specifications we include a control for these zoning changes. Details on the construction of these controls are in Appendix A.

We report the results for our baseline specifications on Table 4. The table is organized to report results for our three alternative measures of travel time: average speeds as in Section 2.1 in Cols. 1 and 2, B-spline projected speeds as in Section 2.3 in Cols. 3 and 4, and dummy projected speeds as in Section 2.2 in Cols. 5 and 6. Within each of these, we report the results for Eqs. (4) and (5).

Comparing either Cols. 1, 3 and 5 or 2, 4 and 6 we can see that results for a given specification are similar across alternative estimation methods for the travel time outcome.[17] In all specifications it is also the case that the DID coefficient estimate on the *boro × post* dummy is lower than on the *boro × roll-out* intensity measure, which is what we would expect if a partially-rolled out boro program has a less than full impact on traffic speed. Once the full roll-out of the program is allowed for, we find travel time increases of 8-10% in the boro zone relative to the hail-exclusion zone.[18] To further evaluate the role of timing and pre-trends in our specification, we re-run a version of Eq. (5) in Col. 2 in which the pre-treatment period is defined to start 24 months prior to the actual introduction of the boro program (i.e in August 2011) and we estimate a month-specific $\hat{\beta}_{DID,m}$ coefficient for every month thereafter. Figure 4 plots (in blue) the point estimates and 95% confidence intervals for these coefficients: we can see that there are no pre-trends, as monthly coefficients are flat at zero prior to the actual roll-out of the program. The speed difference between the hail-exclusion and boro zones starts to develop shortly after August 2013, quickly trending upward over the first six months, and then more slowly over the next year. The trend in $\hat{\beta}_{DID,m}$ coefficients tracks

---

the medallion taxi industry. Hamilton and Wichman (2017) find the bikeshare infrastructure reduced traffic in Washington D.C.

[17] We employ an exhaustive set of fixed effects: this results in an $R^2$ well above 0.9 for specifications (1) and (2), but declines to around 0.5-0.6 for projection-based travel times due to higher variance in that outcome variable.

[18] If we had defined "full roll-out" as a ratio relative to a lower denominator (e.g. the average number of boro taxis on the road after a certain period, rather than the maximum of 6,539 taxis) then the estimated impact from the program on traffic speed would be slightly higher, but there would be no effect on the congestion estimates reported in Section 4 below.

the trend in the roll-out of boro taxis: the measure of this roll-out is not used in the estimates plotted in Figure 4, but it is overlaid on the figure for comparison.[19]

In Table 5 we evaluate some alternative specifications to assess our claim that we have estimated an 8-10% causal impact of the boro program on traffic speed (estimates of $\hat{\beta}_{DID}$ can be read equivalently as log increases in travel time or log decreases in speed). Col. 1 presents an estimate in levels, rather than logs, which is statistically significant and consistent with our baseline results: at the sample average of 0.182 seconds per meter (i.e. 12.32 miles per hour) this estimate represents a 7.2% decrease in speed (to 11.44 miles per hour). Col. 2 presents estimates with common time effects (i.e. fully saturated at the run-bin and at the monthly level, but not interacted with runs). Relative to our baseline, this specification allows variation in travel time between runs over time to identify the difference-in-difference estimates.

The major threat to a causal interpretation of the estimates from our research design is that unobservable components of traffic speed could have different trends in the hail-exclusion "control" and boro "treatment" zones, for reasons other than the program's impact. We check against any such linear trends in Col. 3, and find that the estimated impact decreases by only 17% after the inclusion of a linear trend interacted by run and treatment status. Robustness to a difference in unobserved linear trends is a strong test for the validity of a difference-in-differences design (since identification is provided by the timing of the boro program's launch in August 2013 and its subsequent roll-out relative to any linear trend), although this is less the case in a setting such as ours in which all treated units change status at the same time.

We cannot check for robustness against arbitrary, non-linear differences in trends between the treatment and control zones, since the set of these trends contains the roll-out of the boro program that we rely on for identification. We can, however, check the robustness of our estimates against an alternative, well-defined trend that may be a cause for concern. The major recent change to NYC transportation that we have not yet addressed in detail was the growth in ridehail (plotted in Fig. 1), starting with Uber's entry as a black-car service in May 2011. If growth in ridehail played a role in the substantial slowdown of NYC's streets since 2013 (as documented in Appendix C, and for our area of interest by the downward, parallel translation over time of the

---

[19] Close attention to Figure 4 reveals that the "dynamic DID" coefficient estimate spikes in August of each year. These spikes are explained by a seasonal violation of the parallel trends assumption in our DID specification: every August (and to a lesser extent, September) there is a vacation-driven decline in both the population of taxi users and drivers in NYC (see Figure 1 for a monthly time-series of taxi trips that displays negative seasonality in August). The vacation-induced reduction in traffic and increase in speed is stronger south of the hail-exclusion boundary, resulting in the seasonal variation in travel time differences displayed in Figure 4.

speed curves shown in Figures 2 and 3) then it could bias our estimates: although our research design controls for ridehail's potential effect on traffic speed to the extent that this effect was proportional both north and south of the hail-exclusion boundary, differential impacts across zones remain a potential confounder. To address this concern we construct an "aggregate ridehail trend" from monthly ridehail trips, and interact this trend with runs and the treatment zone.[20] In Col. 4 we jointly include the ridehail trend along with a linear trend: we find that our reduced-form estimate of the impact of the boro program is robust to a trending differential unobservable that is not only linear, but is allowed to accelerate after May 2011 at any rate proportional to the growth of ridehail in New York City.

We present Cols 5 and 6 as checks on statistical inference.[21] In Col 5 we present the results from averaging, for each spatial unit, all time periods into a before and an after period. This is clearly not a preferred specification, as it eliminates variation in observables over time (from controls, such as bike lanes, or the identification provided by the gradual roll-out of boro-taxis that was documented in Fig. 4), but it is useful as a check that statistical significance is not an artifact of time series dependence. We then collapse all variation between road intervals into a single segment average for the treatment or control zone, as a further check that inference does not depend on unmodeled spatial dependence along each avenue. Col 6 presents the difference-in-differences estimate from this further step, which averages each avenue into four cells: both time periods vs. the avenue's treatment and control segments. Under this specification, which contains only 62 observations (and a fixed effect for each of 17 avenue runs, of which 16 are included in the control zone and 15 in the treatment zone) we still find a statistically significant 3.8% additional slowdown of the boro zone relative to the hail-exclusion zone control, which in turn slowed down by 5.8%.[22]

In Table 6 we present results under alternative data samples. Cols 1 and 2 break out results into the east and west sides of northern Manhattan: we find a heterogeneous impact of the boro program, with double the travel time increases on the east than on

---

[20] Trip-level reporting by ridehail providers to the TLC started with the second and third quarters of 2014. There is a gap in reporting during the fourth quarter of 2014, and reporting has resumed from 2015 onwards. We interpolate the monthly growth rate for the fourth quarter of 2014, and extrapolate backwards to Uber's launch in May 2011 using the 10.1% monthly growth rate that has been observed for all ridehail providers since the second quarter of 2014.

[21] Standard errors in all other specifications are two-way clustered at the level of run$\times$ bin and run$\times$ month. Statistical significance holds at coarser clusters such as runs.

[22] We omit averaged controls, since at this level of aggregation they become an arbitrary set of free parameters. Our estimate of the $\hat{\beta}_{DID}$ coefficient is still significant and higher in magnitude if we include averages of our controls, or if we restrict our sample to the balanced panel of 14 runs that span both the treatment and control zones. Results employing the B-spline projection travel time outcome are consistent in sign and magnitude, but not significant at this level of aggregation.

the west side. As we will describe below, this result is associated to a larger increase in taxi activity on the east side. Cols 3 and 4 look at narrow event windows around the introduction of boro taxis (6 and 12 months before and after, respectively). These results confirm that the boro program's impact is identified from variation in traffic speed around the roll-out period (as shown previously by the month-level "dynamic difference-in-differences" results plotted in Fig. 4), rather than long-run trends or events outside the period in which the program was introduced. In particular, results for both windows exclude a city wide-reduction in the speed limit from 30 mph to 25 mph, which took place on November 7, 2014.[23] Speed limits were changed along the entire length of the avenues in our study, so our baseline specifications already control for avenue-level effects through the monthly time-effects $\delta_{rm}$ at the level of each run. Results from Cols. 3 and 4 further confirm that the speed limit change does not introduce a violation of the parallel-trends assumption.

The specifications in Cols. 5-7 are presented as a check for spatial spillovers over the treatment boundaries. Some spatial trends are in fact present in the speed data: inspection of Figures 2 and 3 (see, in particular, the northbound direction of Broadway in Fig. 2a, as well as 3a and 3g) shows that following the program's roll-out, the speed on some avenues starts to decline in areas neighboring the hail-exclusion to the south. Unlike pre-trends in time, which we would not expect the program to produce, it is reasonable to expect the boro program to produce some form of spatial trend due to spatial spillovers. The channels though which the boro program could produce endogenous spillovers include: i) the direct effect of boro taxis on traffic as they drive south of the boundary to drop off passengers; and the incidence of such travel should diminish with distance to the boundary, ii) the direct effect of yellow taxis (or ridehail providers), which may retrench south of the boundary in response to the increased, localized competition from boro taxis to the north, and iii) an indirect effect transmitted through traffic congestion: a taxi may not only have a direct effect that slows down traffic at its immediate location, but also down the road through the effect of queuing cars, or on adjacent roads through gridlock (Schwartz, 2015).

Spatial trends of this form need not constitute a threat to the detection of an effect from the program, but rather to whether our difference-in-difference strategy identifies the program's average effect. In each of the cases outlined above, a spatial spillover from the program slows down traffic in the area we use as a control, biasing our coefficient

---

[23] The speed limit change was part of the broader "Vision Zero" traffic safety program, announced in January 2014 by NYC mayor Bill de Blasio and rolled-out in stages thereafter. The program consists of a broad set of initiatives intended to eradicate traffic fatalities, including public service announcements, a focus on enforcement of traffic laws, street intersection redesign and the change in speed limits. See www1.nyc.gov/site/visionzero/initiatives/initiatives_archive.page for further details.

estimate downward from the program's average effect. To evaluate the sensitivity of our results to spillovers, in Cols. 5-7 of Table 6 we drop the intervals in the control zone that are 250, 500 or 750 meters immediately south of the boundary. The estimated effect rises as we drop adjacent intervals, and we estimate an effect of 0.089 (i.e. 11% higher) if we exclude the 500m adjacent to the treatment boundary, but the sensitivity to this exclusion does not change after this point.

In Col. 8 we employ an alternative specification to directly estimate the third channel for spillovers, i.e. knock-on effects through queuing and road congestion. The degree to which the shock to activity in the boro zone can transmit traffic congestion across the treatment boundary will depend on the direction of traffic: avenues in the downtown direction (i.e. southbound) cannot, by definition, transmit a knock-on effect from queuing traffic across the boundary and can serve as a control group for northbound avenues, in which congestion north of the boundary could spill over into the control zone. We interact our previous difference-in-difference coefficient with an additional difference for the uptown vs. downtown direction of traffic along each avenue and include fixed effects at the level of treatment-zone and month, which absorb the variation that previously identified the difference-in-difference coefficient. Southbound avenues do flow in the direction toward a denser city with slower road speed (as illustrated in the slopes of within-year spatial trends in Figs. 3 and 2), and baseline speed differences could reflect differences in a baseline level of traffic spillovers across the boundary. However, the knock-on effects from this baseline difference are controlled for by $run - bin$ fixed effects, while the addition of boro-zone interacted with time effects in the triple difference specification absorb the average differential trend in speed between north and south of the boundary that is constant across both directions of traffic. We introduce a triple difference coefficient on the interaction of the boro-zone and roll-out intensity measure and an indicator for avenues running in the uptown direction. The coefficient on this interaction is identified, as the boro program rolls-out, from the variation between traffic directions in the within-avenue speed differences across the hail-exclusion boundary: since any knock-on effect would travel backward in the direction of traffic from treatment into control area for uptown runs only, knock-on effects will cause the speed difference across the boundary to be lower for avenues running uptown relative to those running downtown.

The coefficient for the triple difference in Col. 8 is not significant (p-value = 0.145) but its magnitude is consistent with the scale of spillovers that were found in specifications 5-7 by varying the location of the control zone: we estimate a 1.1 percentage point attenuation in the uptown direction, for which road segments in the control zone are subject to spillovers, relative to the downtown direction in which they

are not.[24]

Lastly, we evaluate spillovers through spatial autoregressive models in which we allow for dependence in speed between neighboring road segments. Our aim in estimating a spatial model is to decompose the impact of increased taxi activity due to the boro program into the direct effect on an affected road segment vs. an indirect effect, and in turn use this decomposition to quantify the extent to which spillovers may bias the difference-in-difference estimation of the program's impact. Spatial models have been subject to the criticism (Pinkse and Slade, 2010; Gibbons *et al.*, 2015) that a single reduced form (i.e. the regression of a dependent variable on lagged values of regressors) can be mapped to different sets of structural parameters depending on assumptions on the nature of spatial interactions that are hard to verify (for example, an exclusion restriction on direct effects of lagged regressors distinguishes a pure spatial autoregressive model from one with spatial lags). We do not take a stand in this debate since we are not interested in estimating spatial interaction parameters in their own right. However, there are a couple reasons why a road network is arguably an ideal application for a pure spatial autoregressive model. First, adjacency links are well defined and directed. We consider up to three possible interactions: i) cars can slow down cars that are behind them, so $s_{r,b}$ depends on $s_{r,b-1}$ if $b-1$ is ahead of $b$ in the direction of traffic, ii) $s_{rb}$ depends on $s_{r'b}$ if $r$ and $r'$ are different directions of traffic on the same avenue (note that this interaction is subject to the reflection problem if estimated in isolation) and iii) $s_{rb}$ depends on $s_{r'b}$ if $r$ and $r'$ are neighboring avenues with the same direction of traffic. Second, exclusion restrictions on the structure of spatial lags are reasonable: if a car is slowed down by a double-parked vehicle or a bike lane that is 100 meters up the road, this happens by creating a bottleneck and a slowdown 100 meters ahead that is transmitted down the road through traffic speed, and not through the direct action of double-parking on a car that is 100 meters away.

---

[24] If we isolate the sample to a narrower spatial window around the boundary we estimate a knock-on effect in the range of 1.6 to 2.1 percentage points (for 250 and 500 meter window around the boundary, respectively), both significant at the 1% level. We could ask whether the coefficients estimated from these specifications identify purely the queuing (or knock-on) channel for road congestion. This will depend on whether the other channels we outlined above have a balanced effect over avenues in both directions of traffic. On (ii), we see no reason why competitive retrenchment of yellow taxis or ridehail should be differentially localized to a direction of traffic. On (i), boro taxis do transport passengers southbound across the boundary, but these trips are usually matched by a "dead-head" trip back north to search for the next hail. We cannot use TLC data to quantify the fraction of southbound trips that generate dead-head returns, since boro taxi IDs are not available from the TLC, but our sample of aerial imagery shows that use was balanced in both directions of traffic (we describe this data in Section 4.2). Across 18 images, mostly taken outside peak commute hours, from 10 am to 2 pm, we observe 258 cases of boro taxis south of the East 96th street boundary in our area of interest in the Upper East Side of Manhattan (a density of 9.9 boro taxis per $km^2$), of which 184 were traveling in a north- or south-bound orientation (the remainder were parked or traveling cross-town). Of these, 96 taxis (52.2%) were bearing south and 88 (47.8%) were bearing north.

Following Gibbons *et al.* (2015) we estimate a structural equation of the form $\mathbf{Y} = \rho\mathbf{WY} + \beta\mathbf{X} + \varepsilon$ by directly instrumenting the endogenous, spatial autoregressive term with its reduced form in terms of series of distributed lags for the exogenous variables, i.e. $\mathbf{WY} = \pi_1\mathbf{WX} + \pi_2\mathbf{W^2X} + \pi_3\mathbf{W^3X} + \pi_4\mathbf{W^4X} + \cdots + \nu$, where $\pi_i = \rho^{i-1}\beta$ and $\nu = (\mathbf{W} + \rho\mathbf{W^2} + \rho^2\mathbf{W^3} + \dots)\varepsilon$. In Table 7 we report model estimates using four spatial lags in the first stage and under two alternative spatial weighting matrices: Col. 1 employs a matrix $\mathbf{W_a}$ that includes all the interactions listed above, while the matrix $\mathbf{W_b}$ used for Col. 2 includes only backward effects along a direction of traffic. The estimated coefficient for spatial dependence varies between both models, which affects the precision and the decomposition of program impact. Estimates of the program's total effect on the boro zone (in Col. 1) are precisely estimated and exceed the difference-in-difference estimates by about 2 percentage points.[25] Spatial dependence decays rapidly in this model and spillover effects are small, standing at about 1 percentage point 50 meters across the boundary and quickly vanishing thereafter. Estimates in Col 2 are less precise: although s.e. on the spatial dependence term are smaller in magnitude, the estimated coefficient $\hat{\rho}_b = 0.956$ is closer to unity which results in higher variance for average structural effects, as reflected in the larger bootstrapped confidence intervals for estimated total and spillover effects. The bootstrapped 95% confidence interval for the overall effect is estimated in the range of 5.6% to 6.5%, whereas spatial spillovers are estimated as a 2.68 percentage point slowdown (with a 95% confidence interval of 0.026 to 0.027) at the first 50 meters, vanishing at a slower rate to remain at 0.5 percentage points 750 meters south of the boundary (0.003 to 0.008 confidence interval). The confidence intervals for the average spillover effect from the boro zone into the hail-exclusion zone span a range from 0.1 to 1.0 percentage points across models, and we will employ these magnitudes below to evaluate the robustness of our baseline results to spatial spillovers.

We review the addition of further controls to our baseline specification in Table 8, including types of bike lane and "311" hotline complaints, as well as commercial zoning.[26] The bottom line from the table is that the inclusion of a large set of road

---

[25] If we let $b$ indicate here an individual run and 10 meter bin, the vector of estimated total (direct plus indirect) structural effects for every run-bin is given by $\hat{\mathbf{t}} = \hat{\beta}_{DID}\hat{\mathbf{S}}\mathbf{e}$, where $\hat{\mathbf{S}} = (\mathbf{I} - \hat{\rho}\mathbf{W})^{-1}$ and $\mathbf{e}$ is an indicator vector for the bins in the boro zone. The average direct structural effect is $\hat{\beta}_{DID}\frac{1}{|\mathcal{B}|}\sum_{b\in\mathcal{B}}\hat{\mathbf{s}}_{\mathbf{bb}}$ where $\hat{\mathbf{s}}_{\mathbf{bb}}$ are the diagonal elements of $\hat{\mathbf{S}}$ and $\mathcal{B}$ is the set of bins in the boro zone. The average direct plus indirect effect on the boro zone is $\mathbf{e}'\hat{\mathbf{t}}$ and the indirect effect on the boro zone is the difference between the previous two. Indirect effects on the control zone (in its entirety, or average spillovers over specified segments) are defined analogously by selecting and averaging from the vector $\hat{\mathbf{t}}$.

[26] New York City provides a wealth of urban data to the public, its online portal is opendata.cityofnewyork.us. See Glaeser *et al.* (2015) for a discussion of urban data and empirical research. A common roadblock to the use of urban data in causal research designs is that cities do not always store

level controls has a negligible effect on our estimate of the boro program's reduced-form impact: in Col 1 we present results for our baseline DID specification, but with no controls, and find $\hat{\beta}_{DID} = 0.082$. Column 2 includes a large set of road controls, Col 3 includes a commercial zoning change which came into effect in June 2012, restricting ground floor commercial frontages with the goal of "(maintaining), over time, the general multi-store character (and) promoting a varied and active retail environment" along several avenues in the Upper West Side. The addition of both jointly (presented in Col. 4) reduces the DID estimate to 0.077.[27]

The specification in Col. 2 includes a set of additional, more disaggregated controls of the alternative road uses included in our baseline (Table 4, Col 2), such as four types of bike lane, six categories for "311" complaints and a control both for Citibike stations and the road segment to the south of these. This disaggregation has no effect on the DID estimate, and neither does a full set of interactions (not reported) for the two count variables of potholes and complaints. It is not surprising that some of these controls have no incidence on our estimates: Citibike, in particular, only expanded into our area of study after the launch of the boro program, and by June 2016 had not expanded north of W 110 St or E 96 St. The table also reports on a secondary empirical finding on the effect of bike lanes on speed: although our study is not intended to evaluate the effect of bike lanes on street speeds in New York, and our area of study does not exploit all available variation in the deployment of bike lanes, we find that the introduction of bike lanes in northern Manhattan was correlated with slower street speeds, contradicting a previous report by the NYC Department of Transportation (NYC-DOT, 2014). In our baseline specification we find that avenues become 2.4% slower following the introduction of any bike lane, whereas the breakout across bike lane types in Table 8, Col 2 finds that the effect is monotone in the lane type's utilization of road space: signed routes (which do not employ road space, and consist of signage indicating how cyclists should navigate an intersection) are associated to a marginally significant 1.6% speed increase. We find no effect on wide parking lanes (designed to provide additional space for cyclists), whereas standard bike lanes (which cars can invade, in a traffic violation) are associated with a 1.6% speed decrease, and protected bike lanes (in which, usually, a parking lane is moved inward to separate cars from cyclists) are associated to a 3.4% speed decrease. It might be expected that bike lanes should reduce traffic speed by reducing the maximum throughput capacity available to cars. Speed reductions may be small, however, if the

---

or maintain timestamped versions of the data that they produce, whether from administrative records or urban sensors.

[27] The commercial zoning control is a step function that changes in June 2012 over a large area in the Upper West Side. We include zoning only as a robustness check, rather than in our baseline estimates, since it has a small incidence that may be an artifact of overfitting.

flow of cars decreases due to substitution to other roads or transportation modes such as bicycles or transit.[28] Further, bikelanes may improve traffic if they isolate prexisting cycling from other vehicles.

# 4   The elasticity of congestion to taxi supply

In the previous section we quantified the boro taxi program's impact on traffic speed in northern Manhattan. The program's effect on congestion is a first-order cost, to be evaluated by New York transportation regulators along with the program's transportation benefits such as increased taxi hail availability throughout the five boroughs.[29] In this section we estimate the change in congestion in terms of changes in taxi supply. Our goal is to provide a congestion elasticity that can be applied outside of northern Manhattan to regulation issues in the city more broadly, such as medallion deregulation[30] and the expansion in car-based transportation from "disruption" by ridehail.

TLC trip record data allows for the measurement of taxi activity at a high resolution in space and time, but only data on trip endpoints (pickups and dropoffs) is available throughout the roll-out of boro taxis.[31] Taxi pickups are the closest measure to local supply that is available in the TLC data, as they occur at the locations at which taxis cruise for street-hails. Pickups, however, are an imperfect measure of supply because they arise endogenously from matches between vacant taxis searching for hails and

---

[28] Reduced flows following lane reductions would be consistent with the finding by Duranton and Turner (2011) that vehicle-miles traveled are proportional to highway lanes, although this finding is at the level of metropolitan statistical areas and in the long run.

[29] The TLC has issued two reports on the boro program, containing information on changes in the availability of taxi service outside the "Manhattan Core" as well as some assessment of the program's impact on traffic speed. On congestion, the first report (NYC-TLC, 2013) employs data through October 2013 and provides a table with year-on-year changes in average taxi trip speed for trips between 28 broad subdivisions of the city, using data from both yellow and boro taxis. The results are heterogeneous and inconclusive, and as of October 2013 only 1,128 boro taxis (17.3% of the full roll-out) had provided a trip. The assessment in the second report (NYC-TLC, 2015) consists of the following statement: "*As to congestion throughout all five boroughs outside of the Manhattan Core, average Boro Taxi trip speeds have remained steady over the last year, even as more Boro Taxis have entered into service. Comparing trips completed in January through June across the five boroughs, the average trip speed was 11.2 mph in 2014, compared to 11.3 mph in 2015.*" This assessment is i) restricted to trips from Boro taxis only, ii) an average for most of the city, rather than between areas where the program's incidence may be expected to vary, and iii) uses January to June 2014 as a baseline for comparison, although 5,069 boro taxis were already on the road by June 2014 (3,818 as of January 2014), which is 77.5% (58.4% respectively) of the program's peak roll-out of 6,539 boro taxis in June 2015.

[30] Buchholz (2017) and Frechette *et al.* (2016) evaluate deregulation counterfactuals that do not account for endogenous changes to traffic congestion and related costs.

[31] Medallion and driver identifiers, which allow a researcher to study taxi movements between trips, are only available for yellow taxis and through 2013.

potential passengers attempting to hail taxis from the street curb (and who, on the margin, may choose alternative transportation modes or not to begin travel from a given location). Our interest lies in the effect on congestion from the long term increase in supply, as might result from medallion deregulation or the unregulated entry of a close taxi substitute. We contrast two approaches to estimating a curve for the congestion-supply elasticity.

## 4.1 "Back-of-the-envelope" approach

The elasticity of congestion to supply can be decomposed into an elasticity of congestion to pickups times an elasticity of pickups to supply:

$$\eta_{c,s} = \eta_{c,p} \times \eta_{p,s} \tag{6}$$

and these elasticities may vary by location or location attribute. In this section we estimate the elasticity of congestion to supply in two steps, as suggested by Eq. (6). First, we estimate $\eta_{c,p}$ by exploiting the roll-out of the boro program. We then rescale $\eta_{c,p}$ using a common, "back-of-the-envelope" factor obtained from a proportionality assumption between pickups in our area of study and effective supply throughout the city. We estimate both an average and a curve; the latter is identified from heterogeneous decreases in speed and increases in taxi pickups, driven by variation within the boro zone in proximity to the treatment boundary, as well as proximity to subway stations and major intersections. In Section 4.2 below we address the fact that pickups and supply need not be in proportion to each other.

### 4.1.1 Elasticity of congestion to pickups

We begin by estimating an average of the elasticity of congestion to pickups over the entire treatment zone ($\bar{\eta}_{c,p}$), i.e. we employ the boro roll-out as an instrument for the effect of pickups on travel times. The first stage of our empirical specification is:

$$\log \text{pickups}_{rbm} = \pi_{DID} \text{ roll-out}_m \times \text{boro zone}_{rb} + \pi_x x_{rbm} + \delta_{rb} + \delta_{rm} + \nu_{rbm} \tag{7}$$

and the equation for the second stage is:

$$s_{rbm} = \bar{\eta}_{c,p} \log \text{pickups}_{rbm} + \gamma x_{rbm} + \delta_{rb} + \delta_{rm} + \varepsilon_{rbm} \tag{8}$$

where $\bar{\eta}_{c,p}$ is the congestion elasticity of pickups, and we require the exclusion restriction that, conditional on covariates, any effect from the boro taxi program's roll-out on traffic

speed occurred through the activity of both yellow and green taxis (as measured by pickups) rather than any other channel.[32] The first three columns of Table 9 present the OLS estimate of pickups on travel time (Col 1), as well as the first and second stages (Cols. 2-3), for the entire sample. Columns 4-6 provide estimates for the east side, and Columns 7-9 the west side. OLS estimates of the elasticity are small, in the range of 0.013-0.016. First stage estimates show that the boro program's full roll-out had a substantial impact on taxi pickups north of the hail-exclusion boundary: on the order of a 76% increase for the entire sample, although 45% higher on the east side of Manhattan than the west. The instrumental variable estimate of the congestion elasticity of pickups is 10.6%, or 11.7% on the east and 8.3% on the west side of Manhattan.[33] Since our instrument is a (roll-out intensity-weighted) binary variable, the 2SLS estimator is an (intensity-weighted) Wald estimator and we could read the coefficient for each 2SLS estimate from the ratio of the reduced-form (presented above, in Table 4.2 for the entire sample, and Tables 6.1 and 6.2 for the east and west sides) to the first stage estimates. Although the reduced-form impact of the program on traffic speed was double on the east than the west side, we can see that this was partly due to a differential impact on taxi activity, so the gap between congestion elasticity estimates for the east and west sides is narrower than the gap in the reduced-form impact of the program. Figure F.7 illustrates how the boro program roll-out instrument identifies the effect of pickups on travel time.[34] Pickup levels are correlated with travel times, with both higher on average in the hail-exclusion zone. This correlation is reflected in the low magnitude of OLS estimates, which are driven by small changes over time in location-specific attributes, e.g. urban density and economic activity. The shading on the scatter plot into four cells by treatment status and period allows us to see that following the boro program's introduction there was a substantial increase in taxi activity in the boro zone, and that this occurred along with a substantial increase in travel times (in the control zone, taxi pickups barely changed, and there was a more moderate increase in travel times).

We are interested in estimating heterogeneous effects in terms of location attributes (such as an initial level of supply) so that we can derive a congestion elasticity curve

---

[32] On avenues with two directions of traffic we use a trip's bearing (i.e. angle to the destination) relative to the avenue centerline to classify each pickup as occurring in the avenue's uptown or downtown direction.

[33] Table F.4 presents OLS and 2SLS results using the B-spline projection travel time measures: the estimated congestion elasticity of pickups is higher in the overall results and for the east side, but not the west side. Estimates are less precise and are not significant on the west side.

[34] The figure is a scatter plot of the log travel times over log pickups in our estimation sample, but we have averaged blocks of 10 contiguous 10 meter blocks on a run and within a given month so as to plot a tenth the number of points that are in the estimation sample. Road segments in the hail-exclusion zone are in light orange for the pre- period and dark orange for the post- period, and likewise road segments in the boro zone are in light or dark green. Axes are in log travel time and log pickups, but absolute values for speed and pickups are included for convenience.

and apply it outside of northern Manhattan. Although it is feasible to condition on alternative location attributes (e.g. population density, proximity to transit) we estimate an elasticity coefficient for each 10 meter bin north of the hail exclusion boundary, and we will describe the heterogeneity in these elasticity estimates below in terms of the baseline levels of taxi pickups. We estimate a bin-level congestion-pickup elasticity $\eta_{c,p}(b)$ by estimating Eqs. 4 and 7 with an interaction for 10 meter bin north of the hail-exclusion boundary, and then computing Wald estimates as a ratio of the coefficients for each bin. This procedure yields a distribution of heterogeneous estimates $\hat{\eta}_{c,p}(b)$ for the elasticity of congestion to pickups.[35]

### 4.1.2 Elasticity of pickups to supply: back-of-the-envelope

The simplest approach to computing supply elasticities from pickup elasticities is to assume that pickups and supply vary in proportion to each other. As a benchmark, we rescale the estimates of $\hat{\eta}_{c,p}(b)$ by constant values for $\eta_{p,s}$ obtained by assuming proportionality between levels of pickups and an effective taxi supply. In particular, we assume that the density of vehicles of type $v$ = {yellow, boro} in zone $z$ = {hail-exclusion, boro} and in period $t$ = {Before Aug. 2013, After Aug. 2013} is given by $(1/Area\ in\ km_z^2) \times (Avg.\ medallions\ per\ day_{vt}) \times (Avg.\ hours\ per\ medallion\ per\ day_{vt}/18) \times (Pickups_{vzt}/Total\ pickups_{vt})$. Vehicle densities obtained from this back-of-the-envelope formula are displayed in Table 10, Panel A.[36] We then rescale $\hat{\eta}_{c,p}(b)$ by $\bar{\eta}_{p,s}^{BoE}$ (i.e., the ratio of the average change in our "back-of-the-envelope" measure taxi supply for both yellow and boro taxis over the average growth in pickups) to obtain $\hat{\eta}_{c,s}^{BoE}(b)$. By construction, all heterogeneous pickup elasticities are rescaled by the same factor. Figure 6 plots the set of impact estimates in blue, against baseline levels of taxi pickups prior to August 2013, along with a local polynomial regression and a bootstrapped 95% confidence interval. We discuss this curve below.

---

[35] We restrict this analysis to the east side of Manhattan due to data acquisition and processing costs for the sample of aerial imagery that we will describe below.

[36] Averages of monthly statistics are obtained from the TLC's aggregated monthly reports at nyc.gov/html/tlc/html/technology/aggregated_data.shtml, since vehicle identifiers that would allow for the computation of daily or hourly vehicle utilization are not available for boro taxis or for yellow taxis after 2013. The value of 18 hours in the denominator for vehicle utilization reflects the fact that the modal yellow taxi medallion was employed in two shifts of 9 hours each in 2013. Boro taxis are used less hours in a day then yellow taxis, so adjustment by an hourly utilization rate results in a lower effective supply of boro relative to yellow taxis, given the same number of outstanding medallions. The choice of 18 hours is somewhat arbitrary and affects the levels of vehicle densities, but not rates of change or elasticity factors.

## 4.2 Measuring changes in the spatial distribution of taxi supply with aerial orthoimagery

In this section we develop an approach to measuring supply (and, implicitly, the elasticity $\eta_{p,s}$) that does not require us to assume proportionality between pickups and supply. We seek to avoid this assumption because the ratio of pickups to supply may well change under a large and localized supply shock, i.e. the otherwise unobserved event that allows us to identify the effect of taxis on traffic speed.

Our approach is to directly observe changes in supply by constructing a new dataset of taxi and other vehicle locations over space and time. We acquire aerial orthoimagery for northeastern Manhattan captured over 29 dates, 11 before and 18 after August 2013. We manually digitize, i.e. tag, the observed location of 131,921 vehicles in this imagery.[37] Figure 5 shows the densities of taxi locations on the north-east side of Manhattan before and after the boro program.[38]

Aerial imagery reveals how the supply of taxis reallocated around the hail-exclusion boundary following the introduction of the boro program: yellow taxi density decreased slightly throughout most of the kilometer south of the hail-exclusion boundary. At the boundary itself there has been a spike in supply from boro taxis, but this is almost exactly offset by a retrenchment from yellow taxis. The density of yellow taxis has remained largely unchanged north of the boundary, while the additional supply of boro taxis has led to increases in the taxi density from both types of taxi to average 64.6% over the two kilometers north of the boundary (and ranging from 0.0 to 291.5% growth). We calculate a distribution of heterogeneous elasticity estimates $\eta_{c,s}^{Aerial}(b)$ using the bin-level reduced form changes in speed in the numerator and changes in vehicle densities in the denominator. Since our estimates of changes in speed come from a difference-in-difference specification, we analogously define the denominator of the congestion elasticity term for bin $b$ as $(log\ d_{t',b} - log\ d_{t,b}) - (log\ d_{t',hez} - log\ d_{t,hez})$ where $t$ and

---

[37] In our analysis, however, we only employ 26 scenes through June 2016, because the TLC has anonymized geographic coordinates since the second half of 2016. Sources and methods are detailed in Appendix B. We employ all the aerial orthoimagery available for New York City from all known sources (public or commercial) but one, the exception being a second commercial vendor. Examples of imagery and tagging are displayed in Figures B.1a and B.1b. We evaluated and disregarded satellite imagery of the highest resolution available (Digital Globe WV2 and WV3, Airbus Pleiades, Kompsat-3), which is unsuitable for vehicle roadbed counts due to resolution and visual obstruction from buildings. See Donaldson and Storeygard (2016) for a discussion of satellite imagery in economics research.

[38] We have overloaded the term "density" here, in the sense that the plotted curves are kernel density estimates of observed vehicle locations along the centerlines of Manhattan's north-south avenues, but we rescale the density estimates so that the y-axis indicates the density (in vehicles per $km^2$) that any segment length over the x-axis would mean-integrate to over the width of our area of interest, which is between 1st and 5th Avenues. Rescaling allows us to compare changes in vehicle density along a north-south axis before and after the introduction of the boro program.

$t'$ indicate the average of densities over images before and after the boro program's introduction, and the second difference is in the logs of the densities provided in the hail-exclusion zone rows of Table 10, Panel B. Note that we compute the denominator of congestion elasticity estimates from changes in taxi counts, and not changes in counts for total vehicles on the road. Estimates of bin-specific speed changes are a reduced form of the net impact from both an increased taxi supply and any countervailing substitution, while any local substitution behavior toward private vehicles would partially offset the change that we measure in taxi counts, leading us to overstate the net change in vehicles on the road and understate the congestion elasticity from net changes in vehicles on the road. Our congestion elasticity estimates should therefore be interpreted as a reduced form that includes the adaptation in private driving behavior that took place in the setting of boro taxi deregulation, and therefore understates the structural congestion elasticity of taxi supply that would obtain under a counterfactual in which private car use remains constant.[39] In Section 5 below we describe a methodology to attribute non-taxi car counts to private vs. for-hire-vehicles. Applying this methodology to compute the last two columns of Table 10.B we do not find increased substitution of taxis for private cars in the boro zone, but we do find that the boro zone has seen relatively less growth in for-hire-vehicles.

In Figure 6 we plot in orange the set of heterogeneous congestion elasticities against baseline levels of taxi pickups prior to the boro program (along with a local polynomial regression and a bootstrapped 95% confidence interval). The gap between the congestion elasticity curve estimated from aerial imagery and the back-of-the-envelope curve arises precisely due to the variation in the pickup-to-supply elasticity that aerial imagery is intended to control for: the ratio of the growth in pickups relative to the growth in supply has been larger in areas that were previously less well served with taxi supply, i.e. had lower baseline taxi density. The narrowing gap at higher levels of density can be explained if – as we would expect – the match efficiency between taxis and potential passengers increases with density. Accordingly, the back-of-the-envelope estimate derived from the number of pickups (i.e. matches) does a better job of approximating changes in supply at higher densities.

Employing our preferred aerial-imagery measures of supply, we find that the

---

[39] We are unable to estimate a congestion curve for total car counts because some intervals slowed down yet show infinitesimal changes in total car counts, leading to a high variance in elasticity estimates: 10% of the area north of the boundary saw a change of less than 1% in total car counts, whereas the smallest bin-level change in taxi supply is a 12.8% increase. The ratio of the reduced-form impact estimate (an 8.0 percentage point slow down) to the differences in log total vehicle densities (an 8.7 percentage point difference-in-difference growth in total vehicle density, most of which is driven by growth in boro taxis) yields an average travel time to vehicle density elasticity of 0.91.

congestion elasticity of taxi supply averages 0.2 and is at 0.3 at the 90th percentile of the curve, as the curve increases with density and is somewhat convex. We highlight our congestion elasticity estimates at the 90th percentile of baseline taxi pickups because areas with higher taxi activity in our sample are the most comparable to average levels of taxi activity in midtown Manhattan.

# 5 Application: the role of ridehail in the slowdown of NYC traffic

In this section we apply our estimates of the congestion elasticity of taxi supply to explain the substantial slowdown of New York City since 2013. First, we provide descriptive evidence on the depth, timing and extent of the traffic slowdown throughout the city's streets and highways since 2013. Next, we discuss the two existing studies that evaluate the effect of ridehail on traffic congestion in the city, and we complement our assessment of these studies with evidence on traffic speed and vehicle use. We then answer a simple accounting question: given our estimates for the congestion elasticity of taxi supply, could the city's slowdown be accounted for by the additional supply of for-hire vehicles that was enabled by ridehail applications (e.g. Uber, Lyft, Via, Juno and Gett)? To answer this question, we employ aerial imagery counts to estimate the growth in the supply of for-hire vehicles within an area of midtown Manhattan, as well as measure substitution from private vehicles. We find that most of the observed slowdown in midtown Manhattan can be explained by growth in the supply of for-hire vehicles.[40]

Figure 1 shows that the travel time of the median yellow taxi trip has increased substantially since 2013: after remaining flat at an average 5.1 minutes per mile from June 2009 to June 2013, from 2013 onward the median travel time started to rise and has exceeded 6 minutes per mile since the second half of 2016.[41] Median or average travel

---

[40] To our knowledge, our study is the first to quantify growth in the supply of vehicles on the road due to ridehail, and to provided direct (i.e. non-survey) evidence on substitution from private vehicles. Uber has provided academics with data for the purposes of studying the value of the platform to consumers and workers, e.g. Cramer and Krueger (2016), Cohen *et al.* (2016), Hall and Krueger (2016), Angrist *et al.* (2017), Chen *et al.* (2017), Castillo *et al.* (2017) and Hall *et al.* (2017). In particular, Castillo *et al.* (2017) illustrate how dynamic pricing can allow for increased density of Uber vehicles, increasing Uber's efficiency by reducing travel to (and time to) pickup. The paper does not address the impact of Uber on road use or speed. To date, Uber has not provided access to data for the study of congestion externalities or the degree to which ridehail complements or substitutes transit or the use of private vehicles. Outside of a data agreement, Ge *et al.* (2016) find evidence of racial discrimination on the platform.

[41] The same pattern shows up in survey responses from the US Census' American Community Survey (ACS). Manhattan residents reported that travel time to work by car remained approximately constant between 2009 and 2013, but increased by 2.75 minutes (7.6%) from 2013 to 2016.

time over millions of monthly trips could be subject to selection from changing patterns in the use of taxis: congestion could possibly remain constant while passengers choose to take taxis on more congested roads, driving up the median travel time.

To condition on possible changes in travel patterns over space, the plots in Figure C.2.(a)-(c) show time series for selected percentiles of taxi travel time per mile during the month of June, with each line tracking a percentile for a particular "taxi-zone" pair within midtown Manhattan.[42] Percentiles of the travel time across most origin-destination pairs remained flat until June 2013 and have increased thereafter. Figure C.2.(d) summarizes the variation between June 2013 and June 2016: across 342 origin-destination cell-pairs within midtown Manhattan every percentile has shifted upward on average; the median and 10th percentile of travel time increased in 98.9% of all pairs, whereas the 90th percentile increased in 95.3% of pairs. The median travel time has increased by 15.2% on average across all origin-destination cell pairs in midtown. We describe congestion in midtown for the purposes of our accounting exercise but while midtown slowed down by more than average, it is not unusual: extending the previous comparisons to all taxi-zone pairs with more than 5 trips in both June 2013 and June 2016, we find that the median taxi trip slowed down by more than it did on average in midtown across 34.4% of the cell-pairs in the city. Figure C.3 reports on speed changes using a data source that is novel to our paper: pair-linked event data from a network of EZ-pass sensors throughout highways and expressways in the city. There is a gap in the data around 2014, but there has been an evident slowdown since 2013 throughout the entire distribution of highway speeds (fig. a), throughout the day (b), and throughout the city's network of highways (contrasting (c) and (d)).[43]

The fact that the speed of traffic in New York City has declined substantially in recent years has been reported previously in the media and through aggregate statistics in city transportation reports.[44] However, there is no prior academic research on the timing and scale of the slowdown, or credible empirical evidence on its causes. In January 2016 the Office of the Mayor issued the ad-hoc *For-Hire-Vehicle Transportation Study*" (NYC, 2016), which concluded that "*reductions in vehicular speeds are driven primarily by*

---

[42] "Taxi-zones" are polygonal cells defined by the Taxi and Limousine Commission, and are the finest spatial unit at which trip origination data is provided by ridehail apps. From July 2016 onward the TLC has also started anonymizing individual taxi trip records to the taxi-zone level. There are 19 taxi-zones in midtown Manhattan and 263 in all of the city.

[43] While the NYC Department of Transportation exposes the data to the internet as a real-time feed (see Data Appendix A), the DOT has claimed in correspondence with us not to have archived it. We have archived the data since 2015, and data from three months including June 2013 was kindly made available by Prof. Tomonari Masada of Nagasaki University, who archived it for unrelated research.

[44] Examples include Fitzsimmons and Hu (2017) and Aaron (2015). NYC-DOT (2016) reports a 12% slowdown between 2010 and 2015 in the annual average of taxi trip speed in Manhattan below 60th Street, and a 20% slowdown in a "Midtown Core" area.

*increased freight movement, construction activity, and population growth. (...) E-dispatch (...) did not drive the recent increase in congestion in the CBD.*" The report fails to meet modern standards for identification and there is evidence that it was produced under strong industry lobbying.[45] A second report (Schaller, 2017) cautions that vehicle miles traveled in the city are on the rise due to ridehail.[46] As corroborating evidence, we estimate time series for VMTs per day, making explicit methodological decisions to address censoring in the data but remaining agnostic on the distribution of VMTs between traditional car services and ridehail (see Appendix E). We plot time series for estimated VMTs in Figures C.4d and C.4e. We find that the sum of taxi (yellow plus boro) and FHV miles increased by 886 million miles (34.6%) between 2013 and 2016. Our results are broadly consistent with Schaller (2017), although that report may understate growth in miles through 2016 as well as ridehail's impact through 2015.[47]

In addition to documenting the extent and timing of speed changes and vehicle use through data from taxi meters, EZ-pass and odometer inspections, our contribution to the study of the causes of New York City's slowdown consists of i) measuring the growth in the supply of for-hire vehicles on the road, and ii) applying our estimate of

---

[45] During the summer of 2015, NYC Mayor Bill de Blasio suggested capping growth in for-hire vehicles. In the words of former Uber lobbyist Bradley Tusk, "*we were able to, through a really aggressive campaign, beat back completely (...) some limitations on Uber's growth. (...) We ran $4 million in TV spots. We did radio ads. We did direct mail. We had digital ads. We mobilized our customers (...) We had five different lobbying firms. We worked every single editorial board in the city. We worked the columnists and the pundits. It was just an all-in, 24-hour-a-day campaign*" (quoted from Mehta, 2016). The claim that ridehail did not cause congestion is made by incorrectly equating trip counts to vehicle supply: "*increases in e-dispatch trips are largely substituting for yellow taxi trips in the CBD. Because these e-dispatch trips are substitutions and not new trips, they are not increasing VMT (Vehicle Miles Traveled).*" Congestion is attributed to construction and pedestrians by appealing to correlation with city-wide growth rates in these activities since 2009, a baseline year affected by economic recession.

[46] Using odometer inspection data from for-hire vehicles and taxis, and under some explicit assumptions on private car use and substitution, Schaller (2017) estimates that ridehail led to an additional 600 million vehicle-miles traveled in 2016 relative to 2013, a 27.1% growth over yellow taxi and FHV miles in 2013. Schaller's analysis requires unstated assumptions to handle the fact that vehicle mileages are censored at the last available inspection date, and to allocate flows of miles at the VIN level to stocks of ridehail vs. traditional car services.

[47] Following an initial freedom-of-information request we found that the odometer data that was provided to Schaller contained gaps. Consultation with the TLC allowed us to obtain additional inspection data. More substantively, Schaller deducts the decline in yellow taxi VMTs from his gross estimate of ridehail VMTs, under the assumption that all losses in taxi miles were substitution and not additional miles created by ridehail. However, the report does not track VMTs by boro taxis, which as Figure C.4d shows more than offset the declines in yellow taxi VMTs though the first half of 2016. Since Schaller (2017) implicitly assumes no substitution from yellow to boro taxis, any degree of actual substitution would imply that the estimate of ridehail's growth is biased downward. The report also claims to be consistent with the finding in NYC (2016) that ridehail was not a major source of congestion through the first half of 2015. Unlike the rest of the report, however, this claim is based on growth in trip counts rather than VMTs. Analyzing VMTs for the same period as NYC (2016), we find that VMTs from yellow taxis plus FHVs increased 8.4% between June 2013 and June 2015, and by a further 17.8% between June 2015 and June 2016 (15.0% and 24.0%, respectively, if VMTs from boro taxis are included).

the marginal congestion of taxi supply to evaluate whether increases in vehicle supply are consistent with the observed slowdown.

There are challenges to the use of aerial imagery to count supply on the road. Due to the cost of digitizing the imagery we restrict our analysis to an area on the east side of midtown Manhattan, delimited by 1st and 6th avenues and by 38th and 57th streets. We must also rely on a small sample of historical images captured before and after the introduction of ridehail. As in Section 4.2, we compare periods before and after August 2013: comparisons between these two periods are differences in means over a sample of 26 images, 11 before and 15 after August 2013 (details in Appendix B). A further methodological challenge is that aerial images do not reveal whether observed cars are private or for-hire vehicles. We address this shortfall in the data by counting (in addition to taxis and trucks) the cars that have a black exterior color separately from cars of any color other than black. Counting by color was motivated by a prior that black is the most popular color among for-hire vehicles in New York City, as well as a growth in the share of black cars over successive aerial images that is evident to the naked eye. We then obtained current and historical snapshots of the vehicle registration data for every vehicle in the state from the New York Department of Motor Vehicles. The data contains exterior paint color and county of registration for almost all vehicle identification numbers (VINs). We calculate the share of vehicles with a black exterior paint color among those with an active NY state registration and registered as for-hire vehicles with the Taxi and Limousine Commission ($\alpha_t^{b,F}$). Equivalently, we calculate $\alpha_t^{b,P}$ for private cars (i.e. non-TLC registered) in NYC. Black-paint shares averaged 20.9% for private cars and 73.0% for FHVs in our period.[48] For each image we obtain a pair $(c_i^b, c_i^{nb})$ of car counts by color. If we are willing to assume that the paint color shares of cars counted in our midtown area of interest are proportional to color shares in the vehicle registration data for New York City, then we can derive an estimate of the otherwise unobserved counts for private and for-hire vehicles $(\widehat{c}_i^P, \widehat{c}_i^F)$ in midtown by inverting

$$
\begin{bmatrix} c_i^b \\ c_i^{nb} \end{bmatrix} = \begin{bmatrix} \alpha_t^{b,F} & \alpha_t^{b,P} \\ 1 - \alpha_t^{b,F} & 1 - \alpha_t^{b,P} \end{bmatrix} \times \begin{bmatrix} \widehat{c}_i^F \\ \widehat{c}_i^P \end{bmatrix}
\tag{9}
$$

for each image.

Average vehicle densities per $km^2$ were reported earlier in Table 10, Panel B, but we refer now to counts for midtown Manhattan. We find that the number of vehicles per

---

[48] Vehicle counts likely include commuters from outside the city. We cannot trace the origin of the vehicles in our midtown counts to neighboring states and counties, and lack vehicle registrations by color for neighboring states. However, black-paint shares for private vehicles barely change (average 19.2%) if we include registrations from neighboring Nassau and Westchester counties in NY state.

$km^2$ increased by 14.1% from the 11 images prior to the 15 images after August 2013. We underscore that due to the small size of our sample and the variance over images, the estimates are imprecise: although 14.1% growth is an economically significant magnitude, it is not statistically significant. We do find a statistically significant 11.8% decline in the number of yellow taxis. We also find a 42.5% increase in the number of cars, which breaks down into a 122.7% increase in black cars and a 9.3% increase in non-black cars. Using the share of car colors in the general population of NYC vehicles, we estimate that private cars on the road decreased by 6.8%, whereas the density of FHVs increased by 222.9%. The increase in FHVs from 112.5 to 363.3 per $km^2$ more than offset the drop in 62.5 observed taxis per $km^2$: the sum of taxis plus FHVs on the road in midtown has increased 30.5% in the average of aerial images observed over the past three years, relative to the four years earlier.

In Section 4 we non-parametrically estimated a congestion elasticity curve for taxi supply that increased in baseline taxi activity. A purpose for estimating a curve rather than an average was to extrapolate from the northeast of Manhattan to the denser midtown area: we select an estimated elasticity of 0.304, which corresponds to the 90th percentile of baseline taxi activity. At this value, the observed 30.5% increase in taxi plus FHV density can account for a 9.3% slowdown in traffic in midtown Manhattan. Taking the median change in speed across midtown taxi zones from June 2013 to June 2016 (a 15.2% median slowdown) as a representative value, we find that the growth in the supply of vehicles on the road that was caused by ridehail can explain 61.8% of the traffic slowdown in midtown.[49]

Our application does not establish a causal effect from ridehail on traffic speed. However, it is reasonable to find (given our causal estimates of the congestion elasticity of supply) that the largest change to road transportation in New York City over the past three years can account for most of the observed slowdown. Our count (and other) data also shed light on some of the alternative causes that have been suggested for the slowdown. We cannot measure the use of the road by couriers and delivery services but, as elsewhere in the city, we find that truck counts have decreased. We count 7.6 boro taxis per $km^2$ after August 2013, which relative to a total count of 1301.8 vehicles suggests that boro taxis' impact on midtown congestion has been negligible. We do not adjust our estimate of the change in vehicle supply for changes in private car use, since adaptation in private use is part of the reduced form impact in our congestion elasticity estimates.

---

[49] We have made some conservative data decisions to arrive at this headline result: our estimates employ average speed measurements as the outcome variable (vs. B-spline projections) and do not adjust for spatial spillovers, both of which would result in higher congestion elasticity estimates. Congestion impact estimates using speed measurement only at the times that correspond to the capture times for the aerial imagery do not significantly affect results (see Table F.5).

However, our aerial counts find evidence of modest substitution. Our estimates of this substitution are not statistically significant, although we emphasize that this is due to our small sample, rather than an insignificant economic magnitude.[50] Bike lanes are also unlikely to play any role in the traffic slowdown within the area of our application in midtown: the area has 46.1 km of roads and 6.9 km of bike lanes, but almost all these bike lanes were already in place by June 2013. The only bike lane expansion over the next three years was the conversion of 489 meters along 1st Avenue from shared to protected bike lanes. This expansion implies a 1.1% change in road exposure (absent a correction for spatial spillovers) to a differential slowdown of which our best estimate is 1.6 percentage points, as reported in Table 8. The Citibike bikeshare system was also already in place in midtown by June 2013.

It is also worth noting that the slowdown in highways and expressways that we document using EZ-pass data is inconsistent with some of the suggested alternative explanations for congestion. Bike lanes, cycling and pedestrians are almost surely unrelated to slower highways. Although courier and delivery services may have led to increased highway use, their impact would be relative to baseline utilization for delivery to brick-and-mortar stores. The channel that NYC (2016) suggests for the impact of delivery services, double-parking, is not relevant on highways either. We have not undertaken a study of highway construction projects in New York City, but the widespread spatial distribution of the highway slowdown seen from Figure C.3c to C.3d suggests that individual construction projects are an unlikely source. On the other hand, we cannot rule out that increases in traffic due to boro taxis, which are a negligible cause of congestion in midtown Manhattan, may have contributed to highway congestion in the outer boroughs.

## 6 Conclusions

In this paper we evaluate the congestion cost of a particular taxi deregulation episode in New York City. We also quantify a long-run traffic congestion externality that was previously unmeasured and yet is of first order importance to the regulation of car-based transportation providers in the city. Additionally, we document that there has been a substantial slowdown in NYC's traffic since 2013, and find that the increase in supply due to ridehail can account for most of this slowdown. This is an important result both

---

[50] There is almost no prior research on substitution patterns between ridehail and other modes. Our results are consistent with an internet survey of ridehail users in seven cities conducted by Clewlow and Mishra (2017), who report that "49% to 61% of ride-hailing trips would have not been made at all, or by walking, biking, or transit."

for New York City and for other cities throughout the world that are assessing the costs and benefits of ridehail and evaluating strategies for its effective regulation.

To execute this study we collect and analyze a large number of sources of urban data, of which some are "big", some have not been collected or analyzed previously, and some are entirely new. The City of New York is a leading example in the practice of making urban data publicly available. However, these efforts are at an early stage: standards have not fully developed, and are often geared toward mobile application developers rather than researchers. Some data remains siloed, and some valuable data is lost when it is deemed ephemeral by internal government users and is not archived. Additionally, changes in technology have led to private firms generating and owning data on their utilization of public goods and congestible resources. Regulators may want to develop frameworks so that businesses that are built on the use of public infrastructure report data on this use. The availability of urban data will increase in the near future, along with the use of internet-connected devices and other urban sensors. The use of methods from empirical economics in the analysis of such data can be expected to increase, motivated by changes to the economic activities that take place within cities (in transportation, these may include ridehail, bike lanes, bikeshare, dynamic tolling and autonomous vehicles). In the future, in-vehicle GPS may allow for first-best remedies such as road-specific congestion pricing – as long as regulators can quantify and price the relevant externalities.

# References

Aaron, K. (2015). If Not Uber, Who's Responsible for This Traffic? *WNYC Broadcast. August 11, 2015*.

Ahlfeldt, G. M., Redding, S. J., Sturm, D. M. and Wolf, N. (2015). The Economics of Density: Evidence From the Berlin Wall. *Econometrica*, **83** (6), 2127–2189.

Akbar, P. and Duranton, G. (2017). Measuring the Cost of Congestion in Highly Congested City: Bogotá.

Anderson, M. L. (2014). Subways, Strikes, and Slowdowns: The Impacts of Public Transit on Traffic Congestion [†]. *American Economic Review*, **104** (9), 2763–2796.

—, Lu, F., Zhang, Y., Yang, J. and Qin, P. (2016). Superstitions, street traffic, and subjective well-being. *Journal of Public Economics*, **142** (Supplement C), 1–10.

Angrist, J. D., Caldwell, S. and Hall, J. V. (2017). *Uber vs. Taxi: A Driver's Eye View*. Working Paper 23891, National Bureau of Economic Research.

Barth, M. and Boriboonsomsin, K. (2008). Real-World Carbon Dioxide Impacts of Traffic Congestion. *Transportation Research Record: Journal of the Transportation Research Board*, **2058**, 163–171.

Buchholz, N. (2017). *Spatial Equilibrium, Search Frictions and Efficient Regulation in the Taxi Industry*. Working paper.

Castillo, J. C., Knoepfle, D. T. and Weyl, E. G. (2017). *Surge Pricing Solves the Wild Goose Chase*. SSRN Scholarly Paper ID 2890666, Social Science Research Network, Rochester, NY.

Chen, M. K., Chevalier, J. A., Rossi, P. E. and Oehlsen, E. (2017). *The Value of Flexible Work: Evidence from Uber Drivers*. Working Paper 23296, National Bureau of Economic Research.

Clewlow, R. R. and Mishra, G. S. (2017). *Disruptive Transportation: The Adoption, Utilization, and Impacts of Ride-Hailing in the United States*. Research Report UCD-ITS-RR-17-07, University of California, Davis.

Cohen, P., Hahn, R., Hall, J., Levitt, S. and Metcalfe, R. (2016). *Using Big Data to Estimate Consumer Surplus: The Case of Uber*. Working Paper 22627, National Bureau of Economic Research.

Cramer, J. and Krueger, A. B. (2016). Disruptive Change in the Taxi Business: The Case of Uber. *American Economic Review: Papers & Proceedings*, **106** (5), 177–182.

Currie, J. and Walker, R. (2011). Traffic Congestion and Infant Health: Evidence from E-ZPass. *American Economic Journal: Applied Economics*, **3** (1), 65–90.

Donaldson, D. and Storeygard, A. (2016). The View from Above: Applications of Satellite Data in Economics. *Journal of Economic Perspectives*, **30** (4), 171–198.

Duranton, G. and Turner, M. A. (2011). The Fundamental Law of Road Congestion: Evidence from US Cities. *American Economic Review*, **101** (6), 2616–2652.

Farber, H. S. (2015). Why you can't find a taxi in the rain and other labor supply lessons from cab drivers. *The Quarterly Journal of Economics*, **130** (4), 1975–2026.

Fitzsimmons, E. G. and Hu, W. (2017). The Downside of Ride-Hailing: More New York City Gridlock. *The New York Times. March 6, 2017.*

Frechette, G. R., Lizzeri, A. and Salz, T. (2016). *Frictions in a Competitive, Regulated Market Evidence from Taxis*. Tech. rep.

Gao Hodges, G. R. (2012). *Taxi!: A Social History of the New York City Cabdriver*. Baltimore: NYU Press.

Ge, Y., Knittel, C. R., MacKenzie, D. and Zoepf, S. (2016). *Racial and Gender Discrimination in Transportation Network Companies*. Working Paper 22776, National Bureau of Economic Research.

Gibbons, S., Overman, H. G. and Patacchini, E. (2015). Chapter 3 - Spatial Methods. In J. V. H. Gilles Duranton and W. C. Strange (eds.), *Handbook of Regional and Urban Economics*, *Handbook of Regional and Urban Economics*, vol. 5, Elsevier, pp. 115–168.

Glaeser, E. L., Kominers, S. D., Luca, M. and Naik, N. (2015). *Big Data and Big Cities: The Promises and Limitations of Improved Measures of Urban Life*. Working Paper 21778, National Bureau of Economic Research.

Greenshields, B. D. (1948). The Potential Use of Aerial Photographs in Traffic Analysis. In *Proceedings of the Highway Research Board*, vol. 27, pp. 291–297.

Haggag, K., McManus, B. and Paci, G. (2017). Learning by Driving: Productivity Improvements by New York City Taxi Drivers. *American Economic Journal: Applied Economics*, **9** (1), 70–95.

— and Paci, G. (2014). Default Tips. *American Economic Journal: Applied Economics*, **6** (3), 1–19.

Hall, J. V., Horton, J. J. and Knoepfle, D. T. (2017). Labor Market Equilibration: Evidence from Uber.

— and Krueger, A. B. (2016). *An Analysis of the Labor Market for Uber's Driver-Partners in the United States*. Working Paper 22843, National Bureau of Economic Research.

Hamilton, T. L. and Wichman, C. J. (2017). Bicycle infrastructure and traffic congestion: Evidence from DC's Capital Bikeshare. *Journal of Environmental Economics and Management*, **Forthcoming**.

Hanna, R., Kreindler, G. and Olken, B. A. (2017). Citywide effects of high-occupancy vehicle restrictions: Evidence from "three-in-one" in Jakarta. *Science*, **357** (6346), 89–93.

Hsieh, C.-T. and Moretti, E. (2017). Housing Constraints and Spatial Misallocation.

Jackson, C. K. and Schneider, H. S. (2011). Do Social Connections Reduce Moral Hazard? Evidence from the New York City Taxi Industry. *American Economic Journal: Applied Economics*, **3** (3), 244–267.

Johnson, A. N. (1928). Maryland Aerial Survey of Highway Traffic Between Baltimore and Washington. In *Proceedings of the Highway Research Board*, vol. 8, pp. 106–115.

Kahneman, D. and Krueger, A. B. (2006). Developments in the measurement of subjective well-being. *The journal of economic perspectives*, **20** (1), 3–24.

Knittel, C. R., Miller, D. L. and Sanders, N. J. (2016). Caution, Drivers! Children Present: Traffic, Pollution, and Infant Health. *The Review of Economics and Statistics*, **98** (2), 350–366.

Lagos, R. (2003). An Analysis of the Market for Taxicab Rides in New York City. *International Economic Review*, **44** (2), 423–434.

Li, S., Purevjav, A.-O. and Yang, J. (2017). *The Marginal Cost of Traffic Congestion and Road Pricing: Evidence from a Natural Experiment in Beijing*. SSRN Scholarly Paper ID 2948619, Social Science Research Network, Rochester, NY.

Liang, J., Gong, J., Sun, J., Zhou, J., Li, W., Li, Y., Liu, J. and Shen, S. (2017). Automatic Sky View Factor Estimation from Street View Photographs—A Big Data Approach. *Remote Sensing*, **9** (5), 411.

Mehta, S. (2016). Meet Uber's Political Genius. *The Vanity Fair Interview. June 17, 2016*.

Molnar, A. and Ratsimbazafy, F. R. (2016). *Substituting Bikeshare for Taxis: Evidence from New York City*. Working paper, Vanderbilt University.

Mundhenk, T. N., Konjevod, G., Sakla, W. A. and Boakye, K. (2016). A Large Contextual Dataset for Classification, Detection and Counting of Cars with Deep Learning. In *Computer Vision – ECCV 2016*, Lecture Notes in Computer Science, Springer, pp. 785–800.

NYC (2016). For-Hire Vehicle Transportation Study.

NYC-DOT (2014). Presentation on "Protected Bicycle Lanes in NYC". Available at nyc.gov/html/dot/downloads/pdf/2014-09-03-bicycle-path-data-analysis.pdf.

— (2016). Mobility Report. October 2016.

NYC-TLC (2013). Hail Market Analysis, available at www.nyc.gov/html/tlc/downloads/pdf/boro_taxi_market_study.pdf.

— (2015). Hail Market Analysis, available at www.nyc.gov/html/tlc/downloads/pdf/hail_market_analysis_2015.pdf.

Pinkse, J. and Slade, M. E. (2010). The Future of Spatial Econometrics. *Journal of Regional Science,* **50** (1), 103–117.

Poco, J., Doraiswamy, H., Vo, H. T., Comba, J. L. D., Freire, J. and Silva, C. T. (2015). Exploring Traffic Dynamics in Urban Environments Using Vector-Valued Functions. *Computer Graphics Forum*, **34** (3), 161–170.

Razakarivony, S. and Jurie, F. (2016). Vehicle detection in aerial imagery: A small target detection benchmark. *Journal of Visual Communication and Image Representation*, **34**, 187–203.

Redding, S. J. and Turner, M. A. (2015). Transportation Costs and the Spatial Organization of Economic Activity. In G. Duranton, J. V. Henderson and W. C. Strange (eds.), *Handbook of Regional and Urban Economics*, *Handbook of Regional and Urban Economics*, vol. 5, Elsevier, pp. 1339–1398.

Reilly, V., Idrees, H. and Shah, M. (2010). Detection and Tracking of Large Number of Targets in Wide Area Surveillance. In *Computer Vision – ECCV 2010*, Lecture Notes in Computer Science, Springer, pp. 186–199.

Sadik-Khan, J. and Solomonow, S. (2016). *Streetfight: Handbook for an Urban Revolution*. New York, New York: Viking, 1st edn.

SANTI, P., RESTA, G., SZELL, M., SOBOLEVSKY, S., STROGATZ, S. H. and RATTI, C. (2014). Quantifying the benefits of vehicle pooling with shareability networks. *Proceedings of the National Academy of Sciences*, **111** (37), 13290–13294.

SCHALLER, B. (2017). *Unsustainable? The Growth of App-Based Ride Services and Traffic, Travel and the Future of New York City*. Tech. rep., Schaller Consulting.

SCHNEIDER, H. (2010). Moral hazard in leasing contracts: Evidence from the New York City taxi industry. *Journal of Law and Economics*, **53** (4), 783–805.

SCHWARTZ, S. I. (2015). *Street Smart: The Rise of Cities and the Fall of Cars*. New York, New York: PublicAffairs, 1st edn.

XIE, L. and OLSZEWSKI, P. (2011). Modelling the effects of road pricing on traffic using ERP traffic data. *Transportation Research Part A: Policy and Practice*, **45** (6), 512–522.

ZHAN, X., HASAN, S., UKKUSURI, S. V. and KAMGA, C. (2013). Urban link travel time estimation using large-scale taxi data with partial information. *Transportation Research Part C: Emerging Technologies*, **33**, 37–49.

# Tables and figures
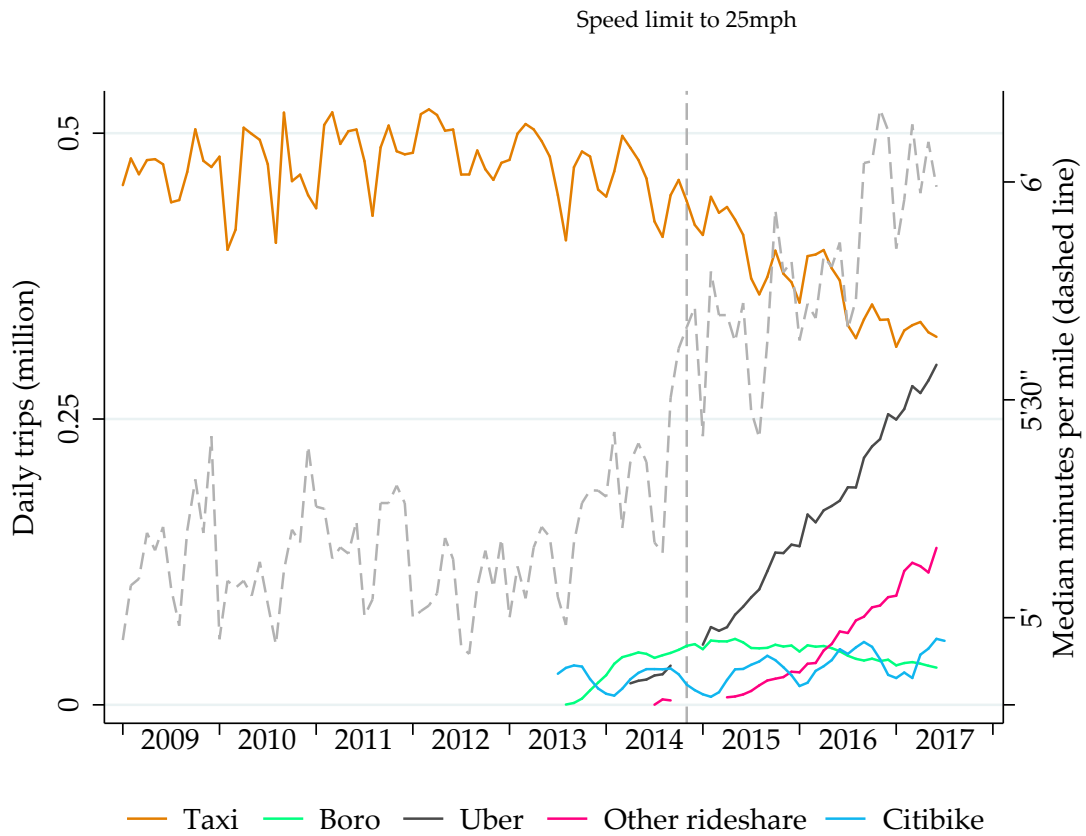


Figure 1: Daily trips in New York City by selected transportation modes, and yellow taxi median minutes per mile. Monthly statistics 2009-2016

Note: Trips from ridehail providers such as Uber and Lyft are available only for Q2 and Q3 in 2014, and from 2015 onwards. Dashed gray line plotted on second axis is the median minutes per mile among all yellow taxi trips in a given month. Vertical dashed line represents the Nov 7, 2014 date on which speed limits were lowered to 25 mph on most city streets under the "Vision Zero" traffic safety initiative.

Table 1: "Taxi race" quasi-experiments: speed comparison between yellow and boro taxis

|  | (12) | (11) | (10) | (9) | (8) | (7) | (6) | (5) | (4) | (3) | (2) | (1) |
|---|---|---|---|---|---|---|---|---|---|---|---|---|
| Seconds | 7.763 | 7.980 | 6.656 | 6.260 | 6.857 | 6.613 | 8.512 | 10.88 | 14.09 | 16.19 | 12.22 | 10.86 |
|  | (3.633) | (3.655) | (3.580) | (3.737) | (3.982) | (4.284) | (4.611) | (4.674) | (5.258) | (6.154) | (7.094) | (6.812) |
| log($Seconds$) | 0.0220 | 0.0237 | 0.0148 | 0.0133 | 0.0129 | 0.0106 | 0.0140 | 0.0256 | 0.0373 | 0.0446 | 0.0351 | 0.0252 |
|  | (0.0171) | (0.0171) | (0.0161) | (0.0169) | (0.0177) | (0.0193) | (0.0216) | (0.0168) | (0.0187) | (0.0218) | (0.0265) | (0.0245) |
| Seconds-per-meter | -0.0805 | -0.0808 | -0.319 | -0.340 | -0.372 | -0.416 | -0.508 | 0.00379 | 0.00542 | 0.00621 | 0.000126 | 0.00289 |
|  | (0.396) | (0.399) | (0.342) | (0.365) | (0.398) | (0.444) | (0.511) | (0.0221) | (0.0260) | (0.0315) | (0.0428) | (0.00686) |
| Race FE | Y | Y | Y | Y | Y | Y | Y | Y | Y | Y | Y | Y |
| Observations | 1,280 | 1,270 | 1,220 | 1,146 | 1,050 | 940 | 816 | 704 | 598 | 494 | 362 | 234 |

Note: All specifications are "taxi race" regressions in which the only regressor is a binary indicator for the boro taxi in a taxi pair, and all between-variation is absorbed by a fixed effect per taxi race, as in a standard "twins" specification. Rows indicate the outcome variable. Columns indicate the number of minutes difference in the pickup time that are allowed for a pair of taxi trip records to be classified as a "taxi race," so sample size increases as this threshold is relaxed. Standard errors clustered at the "race" level. Results are unchanged if controlling for remaining within-experiment variation in observables, such as a "pole position" effect, number of passengers or the residual variation in trip distance on the taxi meter, in the two specifications where the outcome is in units of time rather than a rate of change.

Table 2: Seconds-per-meter for within-avenue taxi trips,
Northern Manhattan, Jan 2009 to Jun 2016

|  | N | Mean | Median | Std Dev | Min | Max |
|---|---|---|---|---|---|---|
| West End Northbound | 262,340 | 0.223 | 0.199 | 0.127 | 0.024 | 6.37 |
| West End Southbound | 379,378 | 0.200 | 0.181 | 0.112 | 0.027 | 8.21 |
| Broadway Northbound | 1,068,259 | 0.205 | 0.181 | 0.130 | 0.026 | 10.90 |
| Broadway Southbound | 1,027,907 | 0.212 | 0.187 | 0.134 | 0.025 | 11.18 |
| Amsterdam Northbound | 514,332 | 0.148 | 0.125 | 0.119 | 0.029 | 12.55 |
| Amsterdam Southbound | 93,688 | 0.238 | 0.204 | 0.166 | 0.040 | 13.40 |
| Columbus Northbound | 1,308 | 0.338 | 0.230 | 0.370 | 0.080 | 4.48 |
| Columbus Southbound | 317,496 | 0.186 | 0.146 | 0.174 | 0.033 | 10.97 |
| Manhattan Northbound | 4,680 | 0.315 | 0.231 | 0.339 | 0.076 | 5.48 |
| Manhattan Southbound | 9,878 | 0.245 | 0.196 | 0.231 | 0.073 | 5.88 |
| CPW Northbound | 132,153 | 0.224 | 0.181 | 0.204 | 0.052 | 8.24 |
| CPW Southbound | 132,674 | 0.230 | 0.189 | 0.203 | 0.039 | 8.85 |
| 5th (S) | 199,727 | 0.242 | 0.191 | 0.209 | 0.035 | 11.26 |
| Madison (N) | 347,121 | 0.209 | 0.163 | 0.190 | 0.035 | 7.74 |
| Park Northbound | 188,904 | 0.238 | 0.196 | 0.193 | 0.026 | 10.16 |
| Park Southbound | 157,976 | 0.281 | 0.224 | 0.243 | 0.030 | 8.39 |
| Lexington (S) | 272,852 | 0.219 | 0.172 | 0.201 | 0.033 | 13.22 |
| 3rd (N) | 440,152 | 0.155 | 0.121 | 0.153 | 0.031 | 14.69 |
| 2nd (S) | 427,408 | 0.194 | 0.153 | 0.174 | 0.026 | 10.07 |
| 1st (N) | 260,863 | 0.157 | 0.119 | 0.160 | 0.031 | 10.29 |
|  |  |  |  |  |  |  |
| Upper East Side | 2,295,003 | 0.201 | 0.157 | 0.189 | 0.026 | 14.69 |
| Upper West Side | 3,944,093 | 0.201 | 0.177 | 0.142 | 0.024 | 13.40 |
|  |  |  |  |  |  |  |
| All | 6,239,096 | 0.201 | 0.171 | 0.161 | 0.024 | 14.69 |

Excluded: Riverside Drive, FDR Drive, Adam Clayton Powell Jr. Boulevard, Malcolm X Boulevard. Statistics are for the seconds per meter, calculated as travel time over the distance along an avenue centerline. The following are statistics in miles per hour for all within-trip observations: the average of 0.201 seconds per meter is the inverse of a speed of 11.13 miles per hour. The maximum is 93.2 miles per hour, the minimum is 0.15 miles per hour, and two standard deviations above the mean is 4.27 miles per hour. Not described in the table above, the 1st and 99th percentile seconds per meter are 0.0789 and 0.762, which are the inverses of 28.4 and 2.93 miles per hour, respectively.

Table 3: Descriptive statistics

|                                                     | Mean    | Median | SD      | Min    | Max   |
|-----------------------------------------------------|---------|--------|---------|--------|-------|
| Seconds per meter (Avg.)                            | 0.182   | 0.182  | 0.039   | 0.104  | 0.554 |
| Seconds per meter (B-spline)                        | 0.102   | 0.0986 | 0.051   | 0.0100 | 0.692 |
| Taxi pickups                                        | 245.666 | 124    | 352.868 | 0      | 7198  |
| 311 complaints                                      | 0.038   | 0      | 0.256   | 0      | 13    |
| 311 complaint: blocked driveway (no access)         | 0.005   | 0      | 0.089   | 0      | 13    |
| 311 complaint: blocked driveway (partial access)    | 0.001   | 0      | 0.038   | 0      | 7     |
| 311 complaint: blocked roadway (construction)       | 0.002   | 0      | 0.044   | 0      | 4     |
| 311 complaint: failed roadway repair                | 0.004   | 0      | 0.074   | 0      | 6     |
| 311 complaint: pothole                              | 0.024   | 0      | 0.194   | 0      | 12    |
| 311 complaint: rough roadway                        | 0.002   | 0      | 0.048   | 0      | 4     |
| Bikelane (any)                                      | 0.089   | 0      | 0.286   | 0      | 2     |
| Bikelane: wide parking                              | 0.020   | 0      | 0.139   | 0      | 1     |
| Bikelane: protected                                 | 0.064   | 0      | 0.245   | 0      | 1     |
| Bikelane: standard                                  | 0.001   | 0      | 0.024   | 0      | 1     |
| Bikelane: signed route                              | 0.005   | 0      | 0.068   | 0      | 1     |
| Citibike station                                    | 0.000   | 0      | 0.008   | 0      | 1     |
| Pothole outstanding                                 | 0.047   | 0      | 0.242   | 0      | 6     |
| Zoning: EC-2/EC-3 districts                         | 0.073   | 0      | 0.261   | 0      | 1     |

Note: Taxi pickups includes all pickups along an avenue, not only within-avenue trips. Bikelane (any) takes a value of 2 at three bikelane intersections.
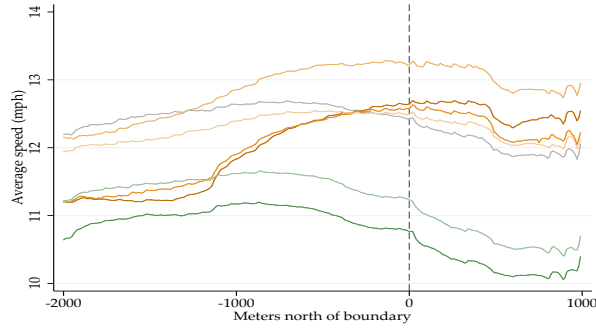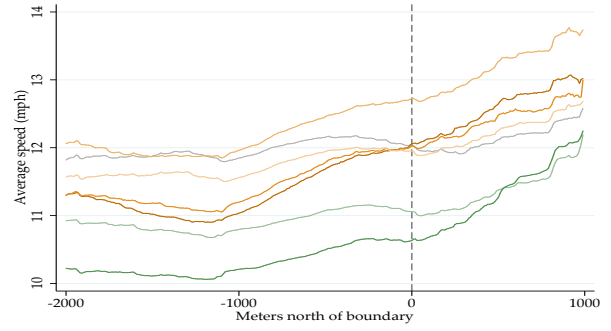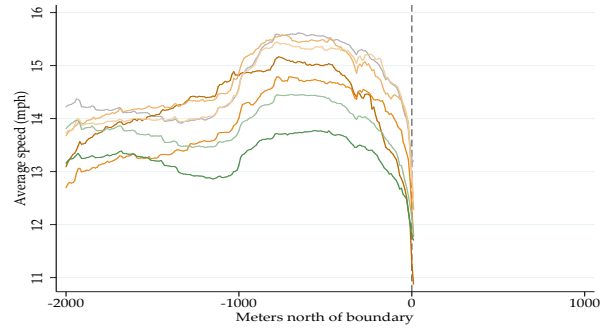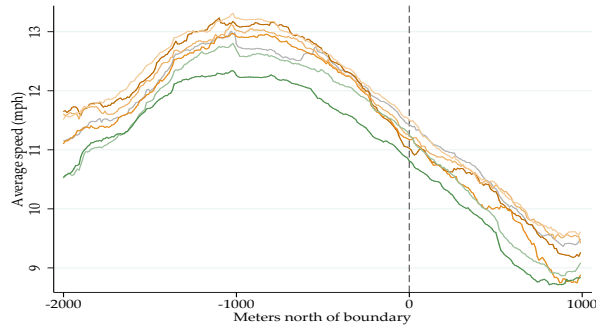
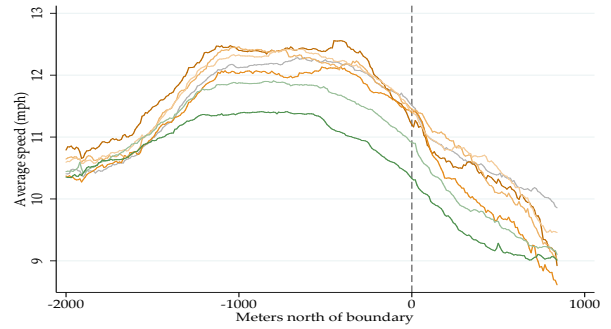(a) Broadway northbound      (b) Broadway southbound
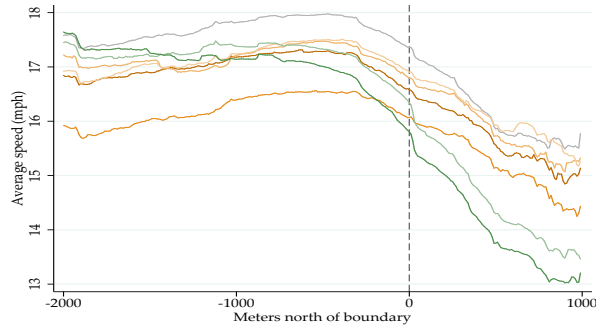
(c) Amsterdam northbound      (d) Columbus southbound

(e) Central Park West northbound      (f) Central Park West southbound

Figure 2: Average travel time at the avenue level, over 10 meter intervals. West side

Notes: Average travel time is computed as the average seconds per meter at the 10 meter interval over all trips that cross the interval. Averages shown here are annual and have been converted to miles per hour. Year is indicated by color and shade, according to the following scheme: years prior to the boro taxi program are indicated in orange, from 2009 (darkest) to 2012 (lightest). 2013 is shown in gray, as program roll-out begins on Aug 8, 2013. 2014 is shown in light green, and 2015 in dark green. 2016 not shown to control for seasonality, since data is only available for the first half of the year. Not plotted: both directions of West End Ave, which are included in regressions but do not identify the coefficient of interest because, like Columbus Ave, they do not cross the hail-exclusion boundary. Manhattan Ave is excluded from plots and regressions because in its short length it does not generate sufficient within-avenue trips to allow for speed measurement.
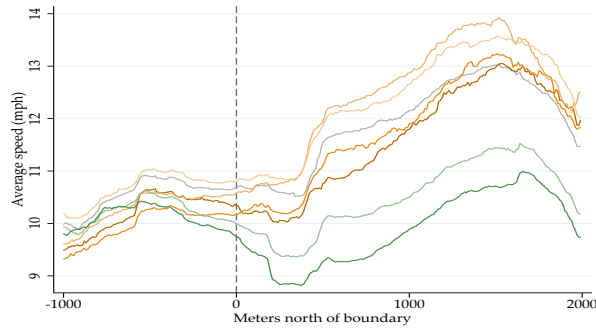
(a) 5th Avenue (southbound)
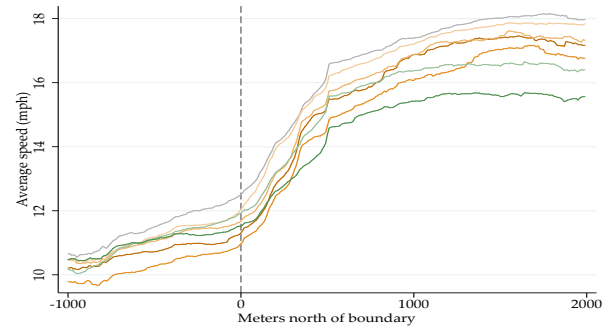
(b) Madison Avenue (northbound)
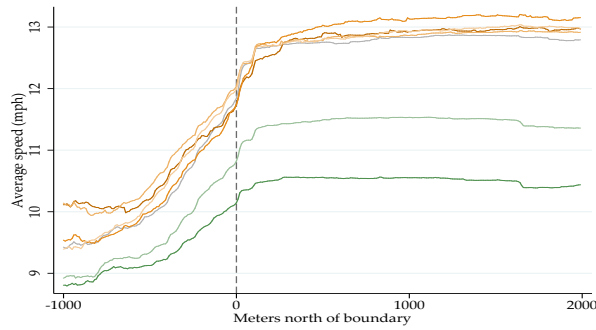
(c) Park Avenue (northbound)

(d) Park Avenue (southbound)
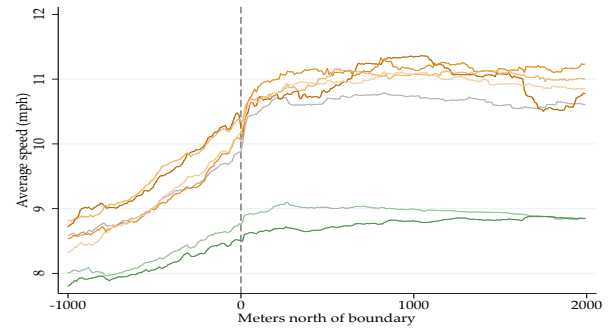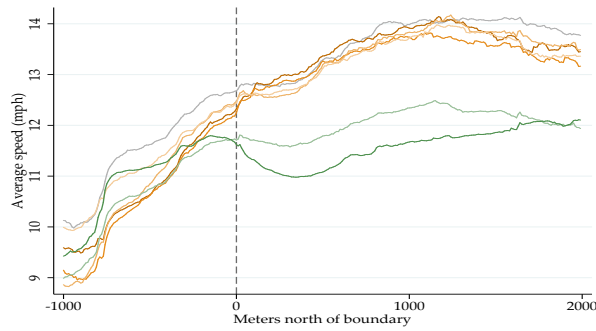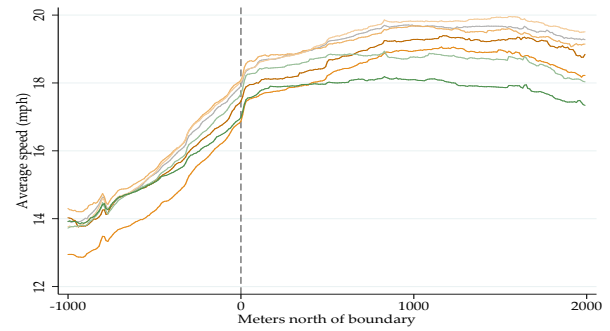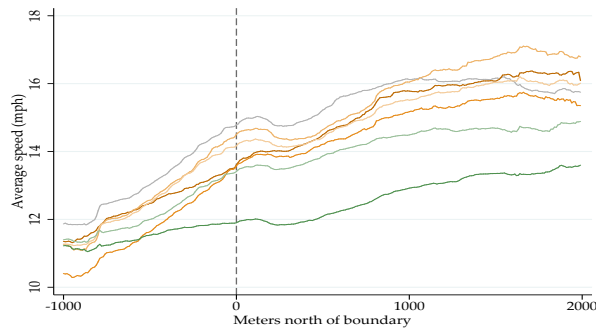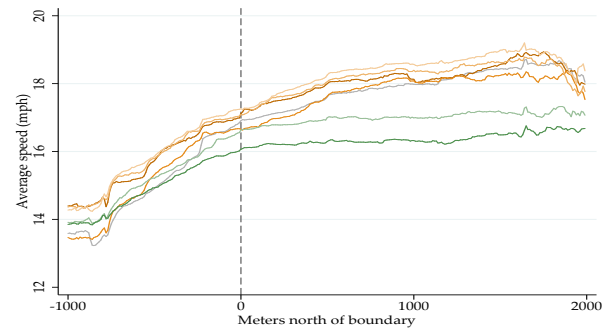
(e) Lexington Avenue (southbound)

(f) 3rd Avenue (northbound)

(g) 2nd Avenue (southbound)

(h) 1st Avenue (northbound)

45

Figure 3: Average travel time at the avenue level (continued). East side

Table 4: Reduced form impact of boro program on congestion.
Comparison across travel time estimation methodologies

| | (1) Log avg. s/m (Treat dummy) | (2) Log avg. s/m (Baseline) | (3) Log Bsp. s/m (Treat dummy) | (4) Log Bsp. s/m (Baseline) | (5) Log est. s/m (Treat dummy) | (6) Log est. s/m (Baseline) |
|---|---|---|---|---|---|---|
| BZ x Post | 0.063 (0.004) | | 0.069 (0.017) | | 0.062 (0.037) | |
| BZ x Roll-out | | 0.081 (0.004) | | 0.101 (0.020) | | 0.083 (0.045) |
| Bikelane | 0.026 (0.004) | 0.025 (0.004) | -0.091 (0.053) | -0.094 (0.053) | 0.084 (0.036) | 0.084 (0.036) |
| Citibike station | -0.018 (0.007) | -0.009 (0.007) | 0.089 (0.036) | 0.103 (0.037) | -0.085 (0.012) | -0.071 (0.015) |
| 311 complaints | -0.000 (0.000) | -0.000 (0.000) | 0.003 (0.003) | 0.003 (0.003) | -0.003 (0.003) | -0.003 (0.003) |
| Potholes | -0.001 (0.001) | -0.001 (0.001) | -0.006 (0.009) | -0.006 (0.009) | -0.008 (0.008) | -0.008 (0.008) |
| Run-bin × Run-my FE | Y | Y | Y | Y | Y | Y |
| Observations | 406260 | 406260 | 406260 | 406260 | 6849 | 6849 |
| $R^2$ | 0.97 | 0.97 | 0.64 | 0.64 | 0.53 | 0.53 |
| $R^2$-within | 0.13 | 0.15 | 0.0015 | 0.0022 | 0.0052 | 0.0058 |

Note: Unless otherwise specified, robust standard errors are two-way clustered at the level of run× bin and run× month. The difference in difference coefficient in the baseline regression (Col. 2, row 2) remains significant at 0.1% with coarser clustering schemes, such as two-way clustering at the level of runs and months (s.e. 0.0151), along any single dimension, or under alternative schemes (and bandwidths) with clustering on the time or time-run dimensions with Newey-West robustness to autocorrelation along the spatial dimension by bin or run-bin. Further evaluation of inference is provided in Table 5, Cols 5 & 6.
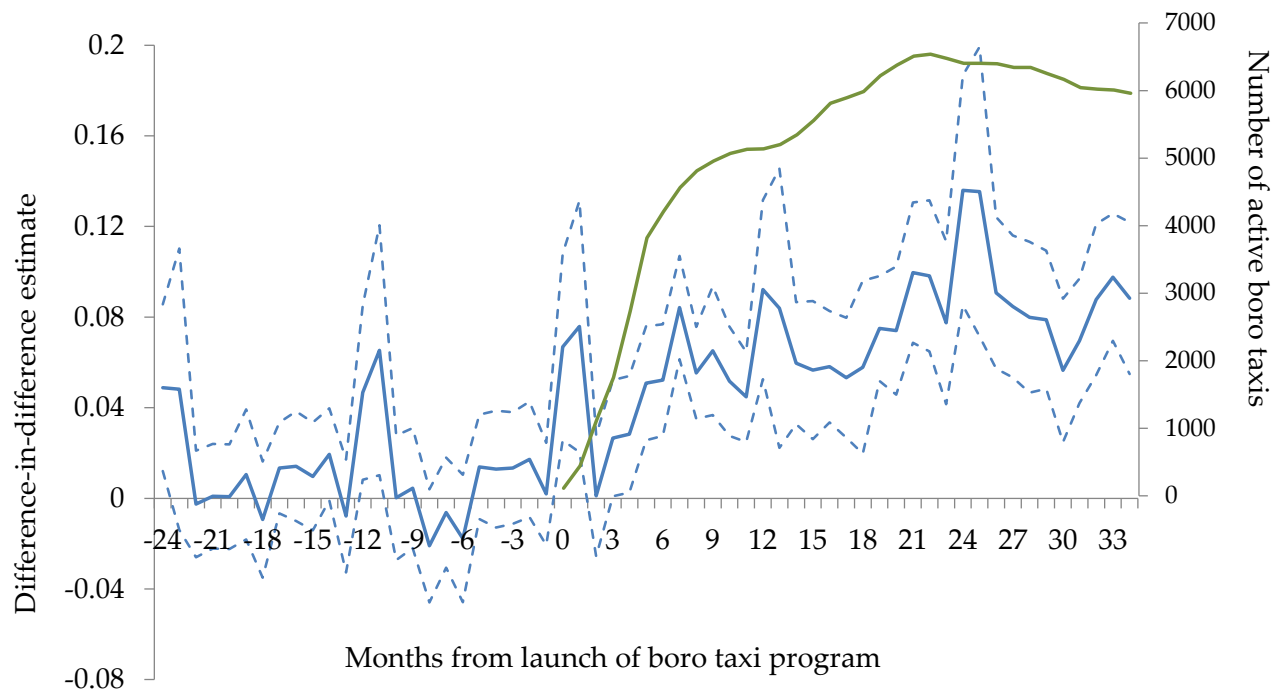
Figure 4: Difference-in-differences estimates of the impact of the boro program, by month

Notes: In green, the number of unique boro taxis active every month, scale on the right axis. In blue, difference-in-differences coefficients and 95% point-wise confidence intervals for standard errors clustered at the run-bin level. The baseline period is defined as the 31 months from Jan 2009 to Jul 2011, thus ending two years prior to the launch of the boro program. A separate coefficient is estimated for every month thereafter. Months are labelled on the plot relative to August 2013. Coefficient estimates are from Eq. (5), and include a fixed effect at the level of the run, 10m bin and month of the year to absorb bin-specific seasonality.

Table 5: Reduced form impact of boro program on congestion.
Alternative specifications

| | (1) Avg. s/m (Levels) | (2) Log avg. s/m (Rect. FE) | (3) Log avg. s/m (Linear trend) | (4) Log avg. s/m (Lin. & rideshare trend) | (5) Log avg. s/m (Aggr. T) | (6) Log avg. s/m (Aggr. T,Run) |
|---|---|---|---|---|---|---|
| BZ x Roll-out | 0.014 | 0.064 | 0.067 | 0.062 | | |
| | (0.001) | (0.005) | (0.007) | (0.007) | | |
| Bikelane | 0.003 | 0.023 | 0.025 | 0.024 | 0.016 | |
| | (0.001) | (0.005) | (0.004) | (0.056) | (0.025) | |
| Citibike station | -0.001 | -0.029 | -0.016 | -0.008 | -0.104 | |
| | (0.001) | (0.020) | (0.007) | (0.084) | (0.106) | |
| 311 complaints | -0.000 | 0.001 | -0.000 | -0.000 | 0.012 | |
| | (0.000) | (0.001) | (0.000) | (0.038) | (0.014) | |
| Potholes | -0.000 | 0.001 | -0.000 | -0.000 | 0.030 | |
| | (0.000) | (0.002) | (0.001) | (0.107) | (0.065) | |
| BZ x Post | | | | | 0.050 | 0.044 |
| | | | | | (0.017) | (0.016) |
| Post | | | | | 0.057 | 0.058 |
| | | | | | (0.012) | (0.012) |
| BZ dummy | | | | | | -0.100 |
| | | | | | | (0.046) |
| Run-bin × Run-my FE | Y | | Y | Y | | |
| Run-bin × my FE | | Y | | | | |
| Run × BZ linear trend | | | Y | | | |
| Run × BZ rideshare trend | | | Y | Y | | |
| Observations | 406260 | 406260 | 406260 | 406260 | 9028 | 60 |
| $R^2$ | 0.96 | 0.93 | 0.97 | 0.98 | 0.98 | 0.85 |
| $R^2$-within | 0.099 | 0.055 | 0.20 | 0.22 | 0.73 | 0.34 |

Note: Unless otherwise stated, robust standard errors are two-way clustered at the level of run× bin and run× month. Estimates with linear and "aggregate ridehail" trends are interacted with the treatment zone and run, but results barely change if interacted at the treatment level only. Estimates in Col. 5 include fixed effects and are clustered at the level of run× bin and run× post, likewise by run× boro-zone and run× post for estimates in Col. 6.

Table 6: Reduced form impact of boro program on congestion.
Alternative samples

| | (1) Log avg. s/m (East) | (2) Log avg. s/m (West) | (3) Log avg. s/m (6m pre/post) | (4) Log avg. s/m (12m pre/post) | (5) Log avg. s/m (cutout 250m) | (6) Log avg. s/m (cutout 500m) | (7) Log avg. s/m (cutout 750m) | (8) Log avg. s/m (DiDiD) |
|---|---|---|---|---|---|---|---|---|
| BZ x Roll-out | 0.100 | 0.049 | 0.042 | 0.077 | 0.086 | 0.090 | 0.086 | |
| | (0.006) | (0.005) | (0.013) | (0.008) | (0.005) | (0.005) | (0.005) | |
| BZ x Roll-out x Uptown | | | | | | | | -0.030 |
| | | | | | | | | (0.006) |
| Bikelane | 0.017 | 0.027 | 0.018 | 0.043 | 0.026 | 0.026 | 0.025 | -0.014 |
| | (0.006) | (0.007) | (0.013) | (0.009) | (0.004) | (0.004) | (0.004) | (0.007) |
| Citibike station | -0.002 | -0.012 | | | -0.005 | -0.001 | -0.001 | -0.019 |
| | (0.010) | (0.003) | | | (0.007) | (0.007) | (0.008) | (0.007) |
| 311 complaints | -0.000 | -0.000 | 0.000 | -0.000 | -0.000 | -0.000 | 0.000 | -0.000 |
| | (0.000) | (0.000) | (0.001) | (0.000) | (0.000) | (0.000) | (0.000) | (0.000) |
| Potholes | -0.002 | 0.002 | -0.001 | -0.001 | -0.000 | -0.000 | 0.000 | -0.001 |
| | (0.001) | (0.001) | (0.002) | (0.001) | (0.001) | (0.001) | (0.001) | (0.001) |
| Run-bin $\times$ Run-my FE | Y | Y | Y | Y | Y | Y | Y | Y |
| BZ-my FE | | | | | | | | Y |
| Observations | 216000 | 190260 | 58682 | 112850 | 374760 | 339840 | 303840 | 200430 |
| $R^2$ | 0.97 | 0.97 | 0.98 | 0.98 | 0.97 | 0.97 | 0.98 | 0.98 |
| $R^2$-within | 0.21 | 0.072 | 0.028 | 0.15 | 0.16 | 0.16 | 0.13 | 0.0098 |

Note: Unless otherwise specified, robust standard errors are two-way clustered at the level of run$\times$ bin and run$\times$ month. Standard errors for the triple-difference estimation in Col. 8 are additionally clustered at the level of boro-zone $\times$ month.

Table 7: Reduced form impact of boro program on congestion.
Spatial autoregressive models for spillovers across the hail-exclusion boundary

| | (1) Log avg. s/m ($W_a$: three adjacencies) | | (2) Log avg. s/m ($W_b$: backward adjacency) | |
|---|---|---|---|---|
| $\rho_a$ | 0.671 | (0.025) | | |
| $\rho_b$ | | | 0.956 | (0.009) |
| | | | | |
| BZ x Roll-out | 0.034 | (0.002) | 0.003 | (0.001) |
| Bikelane | 0.007 | (0.001) | 0.001 | (0.000) |
| Citibike | 0.000 | (0.003) | −0.000 | (0.001) |
| 311 complaints | −0.000 | (0.000) | −0.000 | (0.000) |
| Pothole | 0.000 | (0.000) | 0.000 | (0.000) |
| Run-bin × Run-my FE | Y | | Y | |
| Avg. direct plus indirect effect within BZ | 0.1016 | [0.0998,0.1039] | 0.0613 | [0.0555,0.0649] |
| Avg. direct effect within BZ | 0.0366 | [0.0353,0.0377] | 0.0031 | [0.0022,0.0038] |
| Avg. indirect effect within BZ | 0.0650 | [0.0624,0.0681] | 0.0582 | [0.0532,0.0611] |
| Avg. indirect effect (spillover) on HEZ | 0.0007 | [0.0006,0.0008] | 0.0085 | [0.0071,0.0104] |
| Avg. indirect effect (spillover) on HEZ, first 50m | 0.0102 | [0.0096,0.0110] | 0.0268 | [0.0260,0.0274] |
| Avg. indirect effect (spillover) on HEZ, first 100m | 0.0008 | [0.0007,0.0011] | 0.0215 | [0.0202,0.0229] |
| Avg. indirect effect (spillover) on HEZ, first 250m | 0.0000 | [0.0000,0.0001] | 0.0143 | [0.0122,0.0169] |
| Avg. indirect effect (spillover) on HEZ, first 500m | 0.0000 | [0.0000,0.0000] | 0.0065 | [0.0046,0.0095] |
| Avg. indirect effect (spillover) on HEZ, first 750m | 0.0000 | [0.0000,0.0000] | 0.0050 | [0.0033,0.0078] |
| Observations | 395820 | | 395820 | |
| $R^2$ | 0.991 | | 0.999 | |
| $R^2$-within | 0.72 | | 0.98 | |

Note: Standard errors in parentheses on the reduced-form 2SLS coefficients of the spatial models are robust, two-way clustered at the level of run× bin and run× month, and are displayed on the right of the estimated coefficient. F-statistics from the first stage are 278.3 and 47.4, respectively. For average structural effects (direct and indirect) we display 95% confidence intervals from bootstrapping the structural parameters over 1000 simulations, re-estimating the model and the impact matrix $(\mathbf{I} - \hat{\rho}\mathbf{W})^{-1}$.

Table 8: Reduced form impact of boro program on congestion.
Alternative controls

| | (1) Log avg. s/m (No controls) | (2) Log avg. s/m (Road controls) | (3) Log avg. s/m (Comm. zoning) | (4) Log avg. s/m (All) |
|---|---|---|---|---|
| BZ x Roll-out | 0.082 (0.004) | 0.080 (0.004) | 0.079 (0.004) | 0.077 (0.004) |
| Bikelane: | | | | |
|    Signed route | | -0.016 (0.009) | | -0.016 (0.009) |
|    Wide parking | | 0.012 (0.009) | | 0.014 (0.009) |
|    Standard | | 0.016 (0.006) | | 0.016 (0.006) |
|    Protected | | 0.034 (0.006) | | 0.034 (0.006) |
| Citibike station | | -0.006 (0.002) | | -0.006 (0.002) |
| Citibike (south of station) | | -0.004 (0.008) | | -0.005 (0.008) |
| 311 complaint: | | | | |
|    Blocked driveway (no access) | | 0.002 (0.001) | | 0.002 (0.001) |
|    Blocked driveway (partial access) | | -0.001 (0.002) | | -0.001 (0.002) |
|    Blocked roadway (construction) | | 0.001 (0.001) | | 0.001 (0.001) |
|    Failed roadway repair | | 0.000 (0.001) | | 0.000 (0.001) |
|    Pothole complaint | | -0.001 (0.000) | | -0.001 (0.000) |
|    Rough roadway | | 0.001 (0.001) | | 0.001 (0.001) |
| Pothole outstanding | | -0.001 (0.001) | | -0.001 (0.001) |
| Zoning: EC-2/EC-3 districts | | | -0.020 (0.005) | -0.021 (0.005) |
| Run-bin $\times$ Run-my FE | Y | Y | Y | Y |
| Observations | 406260 | 406260 | 406260 | 406260 |
| $R^2$ | 0.97 | 0.97 | 0.97 | 0.97 |
| $R^2$-within | 0.15 | 0.15 | 0.15 | 0.16 |

Note: Unless otherwise specified, robust standard errors are two-way clustered at the level of run$\times$ bin and run$\times$ month.

Table 9: Wald estimates of the congestion elasticity of taxi pickups

| | (1) Log avg. s/m (OLS) | (2) Log pickups (1st stage) | (3) Log avg. s/m (2SLS) | (4) Log avg. s/m (OLS) | (5) Log pickups (1st stage) | (6) Log avg. s/m (2SLS) | (7) Log avg. s/m (OLS) | (8) Log pickups (1st stage) | (9) Log avg. s/m (2SLS) |
|---|---|---|---|---|---|---|---|---|---|
| Log pickups | 0.015 | | 0.106 | 0.015 | | 0.117 | 0.016 | | 0.083 |
| | (0.001) | | (0.007) | (0.001) | | (0.009) | (0.002) | | (0.011) |
| | | | | | | | | | |
| BZ x Roll-out | | 0.764 | | | 0.860 | | | 0.594 | |
| | | (0.029) | | | (0.038) | | | (0.043) | |
| | | | | | | | | | |
| Bikelane | 0.039 | 0.090 | 0.016 | 0.044 | 0.168 | -0.002 | 0.029 | -0.098 | 0.035 |
| | (0.005) | (0.037) | (0.006) | (0.006) | (0.052) | (0.009) | (0.007) | (0.037) | (0.007) |
| | | | | | | | | | |
| Citibike | -0.035 | -0.087 | -0.000 | -0.043 | 0.008 | -0.003 | -0.017 | -0.228 | 0.006 |
| | (0.008) | (0.101) | (0.013) | (0.010) | (0.135) | (0.019) | (0.004) | (0.102) | (0.011) |
| | | | | | | | | | |
| 311 complaints | -0.000 | 0.004 | -0.001 | -0.000 | 0.004 | -0.001 | -0.000 | 0.006 | -0.001 |
| | (0.000) | (0.003) | (0.000) | (0.000) | (0.004) | (0.001) | (0.000) | (0.003) | (0.000) |
| | | | | | | | | | |
| Potholes | -0.000 | 0.006 | -0.001 | -0.003 | 0.024 | -0.005 | 0.002 | -0.009 | 0.002 |
| | (0.001) | (0.007) | (0.001) | (0.001) | (0.011) | (0.002) | (0.001) | (0.007) | (0.001) |
| Run-bin and Run-m-y FE | Y | Y | Y | Y | Y | Y | Y | Y | Y |
| Sample | All | All | All | East side | East side | East side | West side | West side | West side |
| Observations | 406260 | 406260 | 406260 | 216000 | 216000 | 216000 | 190260 | 190260 | 190260 |
| $R^2$ | 0.97 | 0.95 | 0.94 | 0.97 | 0.95 | 0.93 | 0.97 | 0.95 | 0.96 |

Note: Unless otherwise specified, robust standard errors are two-way clustered at the level of run× bin and run× month. Weak instrument tests are not reported, but the lowest F-stat in the table (for column 9, the West side, Bspline specification) is 35,315. About 1.16% of the 10-meter avenue segments had no taxi pickups within a particular month, so we set the dependent variable at $log(\text{pickups} + 0.1)$. Shifting the dependent variable by 0.01 instead changes the main coefficient in Col (2) from 0.1040 to 0.1012.

## Table 10: Vehicle densities (per $km^2$). Selected areas of interest.

| Panel A: Back-of-Envelope proportional allocation | Yellow taxi | Boro taxi | Taxi Total |
|---|---|---|---|
| **Hail-exclusion zone** | | | |
| Before Aug 2013 | 237.3 | | 237.3 |
| Since Aug 2013 | 232.9 | 1.0 | 233.9 |
| | -1.8% | | -1.4% |
| **Boro zone** | | | |
| Before Aug 2013 | 36.1 | | 36.1 |
| Since Aug 2013 | 32.5 | 36.1 | 68.6 |
| | -10.0% | | 90.1% |

| Panel B: Aerial counts | Cars | Black cars | Trucks | Yellow taxi | Boro taxi | Total | $\widehat{\text{Private}}$ | $\widehat{\text{FHV}}$ |
|---|---|---|---|---|---|---|---|---|
| **Hail-exclusion zone** | | | | | | | | |
| Before Aug 2013 | 264.4 | 108.7 | 82.0 | 247.0 | | 684.1 | 269.8 | 85.3 |
| Since Aug 2013 | 270.4 | 164.9 | 67.1 | 205.4 | 10.1 | 717.8 | 289.6 | 145.7 |
| | 9.7% | 51.7%*** | -18.2% | -16.8%*** | | 4.9% | 7.3% | 70.8%** |
| **Boro zone** | | | | | | | | |
| Before Aug 2013 | 286.9 | 126.0 | 65.1 | 61.8 | | 539.8 | 314.5 | 98.4 |
| Since Aug 2013 | 309.8 | 160.0 | 54.0 | 58.2 | 36.0 | 617.9 | 346.6 | 123.2 |
| | 8.0% | 27.0%* | -17.1% | -5.8% | | 14.5% | 10.2% | 25.2% |
| **Midtown** | | | | | | | | |
| Before Aug 2013 | 370.3 | 153.5 | 86.1 | 530.7 | | 1140.7 | 411.4 | 112.5 |
| Since Aug 2013 | 404.9 | 341.8 | 79.3 | 468.2 | 7.6 | 1301.8 | 383.5 | 363.3 |
| | 9.3% | 122.7%*** | -7.9% | -11.8%* | | 14.1% | -6.8% | 222.9%*** |

Note: "Hail-exclusion" and "boro" zones in both panels designate the area of interest in northeastern Manhattan, all areas described in Appendix B. Rows with percentage changes in Panel B are labeled with stars (* $p < 0.1$, ** $p < .05$, *** $p < 0.01$) for a two-sided difference in means test for the vehicle density (in levels) between the period before August 2013 (11 scenes) and after (15 scenes). Almost all scenes were captured around noon due to favorable lighting conditions, and scenes include both weekday and weekend dates (see Appendix B for details). For each zone, period and vehicle type we estimate a weekend factor and re-weight weekend densities accordingly. Growth rates between the averages of vehicle densities that are weighted or unweighted in this manner are comparable, but unweighted densities are on average 14.3% lower due to lower counts in the weekend sample.
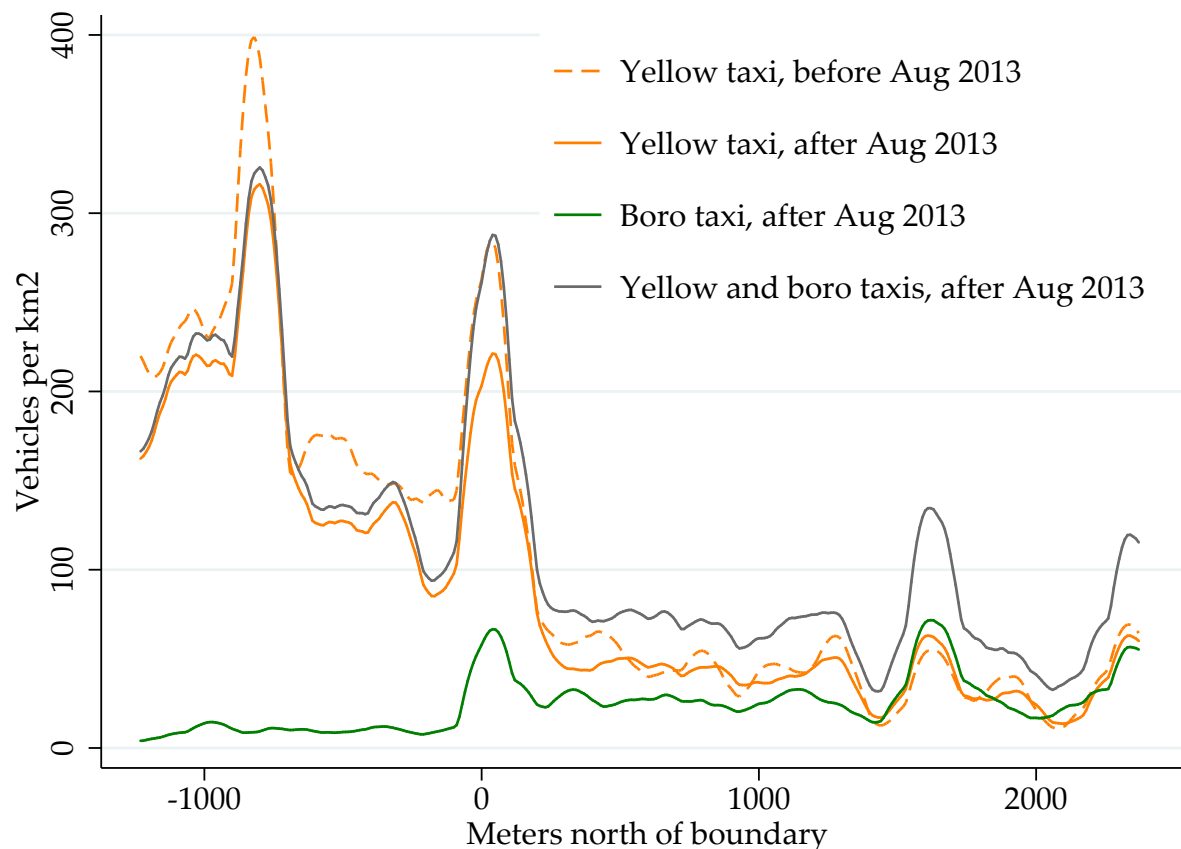
Figure 5: Densities of taxis located from overhead aerial imagery

Note: We plot the densities of the distance between taxis on the road, as located over the area of interest in aerial imagery scenes, and the hail-exclusion boundary. Our area of interest is 4.4 square kilometers (1087 acres) on the east side of northern Manhattan, delimited by 1st Ave and 5th Ave and between East 82nd Street and East 125th Street. We count an average 522.7 yellow taxis per scene (or 118.9 per $km^2$) over 11 scenes prior to the boro taxi program, and plot the density of the locations of these taxis with a dashed yellow line. Following the launch of the boro program we count an average 440.5 yellow taxis and 112.1 boro taxis per scene over 15 scenes through June 2016 (125.6 taxis per $km^2$). We plot the density of the locations of these taxis with solid yellow and green lines. All kernel density estimates are rescaled so that they would integrate to the average number of vehicles per $km^2$ over 1000 meters on the horizontal axis. In this manner, the vertical axis represents a local vehicle "density" (i.e., in terms of vehicles per $km^2$). We plot the sum of the densities for both types of taxis in the post period with a solid grey line to facilitate before-after comparison. All densities are estimated with upper and lower bounds computed by renormalization, and congestion elasticity estimates employ only the range from 1km south to 2 km north of the boundary. Details on aerial imagery are in Appendix B.
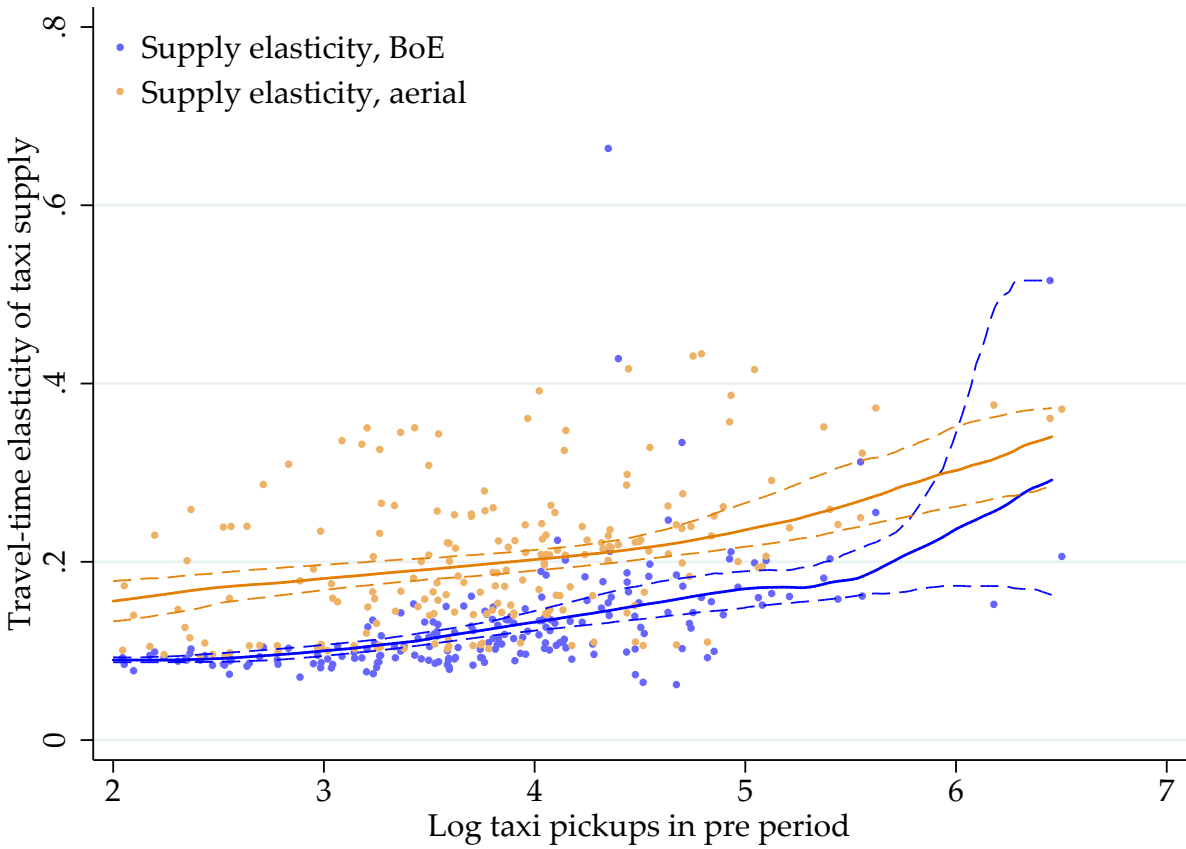
Figure 6: Congestion elasticity curves

Note: Elasticity estimates and curve are in blue for the "back-of-the-envelope" method and in orange for aerial count data. Points represent individual elasticity estimates per 10 meter bin in the east Manhattan boro-zone, placed on the vertical axis, and are sorted on the horizontal axis by the log of average taxi pickups from January 2009 to August 2013. Solid lines are local polynomials for the conditional mean of elasticity on average pickups. Confidence intervals are estimated pointwise, as the 97.5% and 2.5% percentile envelopes from 1000 bootstrapped samples of the local polynomial conditional mean function. Bandwidth for estimation and for every bootstrap sample is selected automatically by a default rule-of-thumb method for the asymptotically optimal constant bandwidth.

# Appendix A   Data sources

**Taxi trips.**   Taxi trip records are from the New York City Taxi and Limousine Commission's Taxicab Passanger Enhancements Project (TPEP) and Street Hail Livery (SHL) Passanger Enhancements Project (LPEP). The paper uses trip records from 2009 through the first half of 2016, obtained from multiple FOIL requests by the authors and as of September 2015 available for direct download from the NYC TLC's website at: nyc.gov/html/tlc/html/about/trip_record_data.shtml. As of the second half of 2016 the TLC has started removing trip endoint coordinates from their data releases, which precludes the street speed reconstruction methods developed in this paper. Data from ridehail and other for-hire vehicle providers was also obtained by FOIL prior to September 2015, and records with the time and "taxi-zone" of pickup are available from 2015 onwards at the TLC website.

**311 complaints.**   Data from reports to New York City's 311 complaint hotline are available at www1.nyc.gov/311/our-data.page. Each record contains the date, location coordinates, and a category classification for the complaint. This paper utilizes all 311 records in northern Manhattan for categories that may be related to the flow of traffic. We count the number of complaints per month and segment of road that fall under the following categories: "Blocked Driveway - No Access," "Blocked Driveway - Partial Access," Street Condition - Blocked - Construction," "Street Condition - Failed Street Repair," "Street Condition - Pothole," and "Street Condition - Rough, Pitted or Cracked Roads."

**Bike lane maps.**   The New York City Department of Transportation provides a shapefile for all bike lanes, including the date of installation or modification, at www.nyc.gov/html/dot/html/about/datafeeds.shtml#bikes. All changes in bike lanes (either new construction or modification) from 2009 through the first half of 2016 are matched to street segments. The various types of bike lane changes in the data include bike-friendly parking, protected paths, signed routes, and standard bike lanes.

**Citibike system.** Bike trip data is from the Citibike system data page at citibikenyc.com/system-data. Data on location and availability of bike stations was archived from the Citibike live station feed, available at citibikenyc.com/stations/json as well as the system data web page.

**Potholes.** Street Pothole Work order data is available at www.nyc.gov/html/dot/html/about/datafeeds.shtml#construction. This dataset contains the reported date and closed date of pothole work orders, identified at the level of street sections between intersections, from 2010 through 2016. Each order may refer to more than one pothole.

**EZ-pass traffic speed.**   Data for traffic sensors in New York City is made available as a real-time feed by the NYC Department of Transportation. A link to the real time feed is available at nyc.gov/html/dot/html/about/datafeeds.shtml#realtime. The NYC-DOT has claimed in private correspondence not to archive the output of this

feed. From May 27, 2013 to August 20, 2013 the feed was continuously archived and kindly made available by Prof. Tomonari Masada of Nagasaki University. Data from April 2015 through August 2015 (and beyond) was continuously archived by *βetaNYC*, a civic technology non-profit, and is available at data.beta.nyc/dataset/nyc-real-time-traffic-speed-data-feed-archived. Data from August 2015 onward was also continuously archived by the authors. Additional snapshots of the data were obtained from archive.org at 11 arbitrary times and dates in 2014 and prior to 2013.

**New York State vehicle registrations**. Obtained from current and previous archived snapshots of the NY State Department of Motor Vehicles database for Vehicle, Snowmobile and Boat registrations, available at data.ny.gov. Data contains county, zipcode, car brand and body type, model year, exterior color and VIN for every vehicle registered in the state of New York.

**Taxi and For-hire-vehicle inspection data**. Obtained by FOIL from the Taxi and Limousine Commission's Vehicle Inspection Program. Data contains odometer readings and inspection dates for yellow taxis (performed quarterly), boro taxis (biannually) and for-hire vehicles (biennially).

## Appendix B  Aerial imagery data

We digitize high-resolution, natural color aerial orthoimagery captured over New York City between 2010 and 2017. Our sample of 29 scenes comes from state and federal government sources (US Dept. of Agriculture, the New York City government), online services (Google, ESRI, Bing), and a commercial vendor (NearMap Ltd.). We have excluded a second commercial vendor (Eagle View Technologies, Inc.) due to licensing cost. Unless otherwise noted below, the nominal resolution for imagery is 15 cm or better. Figure B.1 illustrates this variation in resolution. The sources are:

- 3 scenes from National Agriculture Imagery Program of the US Department of Agriculture (see fsa.usda.gov/programs-and-services/aerial-photography/imagery-programs/naip-imagery for sources). July 10, 2011 (nominal 1m resolution). June 22, 2013 (nominal 1m resolution). May 22, 2015 (nominal 50cm resolution).

- 4 scenes from NY State Digital Orthoimagery Program, distributed by NYC government at maps.nyc.gov/tiles.

- 11 scenes from Google aerial imagery, obtained through the Google Earth Pro desktop application.

- 1 scene from Bing Maps Aerial Imagery layer.

- 1 scene from ESRI World Imagery layer. Resolution is unknown, but is provided at approximately 30 cm.

- 9 scenes from Nearmap Ltd. (© 2017).

(a) Source: National Agricultural Imagery Program. July 10, 2011. Time estimated as 12.30 pm.



(b) Source: Nearmap Ltd. (© 2017). April 12, 2015, within 5 minutes of 2.57 pm.

Figure B.1: Aerial imagery examples. Madison Ave and East 96th Street

Note: the example areas displayed have an area of 0.7 acres, and are intended to illustrate variation in image resolution (1 meter vs. 15 cm). Our area of interest consists of 1087 acres (1.7 square miles) on the east side of northern Manhattan, delimited by 1st Ave and 5th Ave and between East 82nd Street and East 125th Street. Circle icons on the aerial imagery indicate vehicles labeled as taxis (yellow), boro taxis (green), cars (cyan) or black cars (magenta).

On every image we digitize vehicle locations in two areas of interest: i) an area in the northeast of Manhattan that includes parts of the Upper East Side and East Harlem neighborhoods, delimited between 1st and 5th avenues and between East 79th and East 128th streets, and ii) an area in the eastern Midtown district, delimited between 1st and 6th avenues and between 38th and 57th streets (we select the same area as Zhan *et al.*, 2013, which includes the densest zone in midtown Manhattan). We manually tag five classes of vehicles: yellow taxis, green taxis, black cars, cars of any color other than black and trucks, excluding city buses. Yellow and green taxis are tagged anywhere on the roadbed, whether parked or in apparent motion. Cars and trucks are tagged only on traffic lanes. We exclude taxis on parking lots off the roadbed.

A fraction of our aerial images are subject to some degree of road occlusion, i.e. portions of the roadbed are obstructed from view by tall buildings due to the angle at which the camera captured the aerial photography. We impute observations that are missing due to visual occlusion with the following procedure:

1. For any aerial scene $i$ we start with the set of all observed and digitized vehicle locations $L_i$. We refer to any aerial scene with some occlusion as a *recipient* image, and any scene with no occlusions as a *donor* image. We separately process the images that were captured in the period before or after August 2013. For donors, we refer to the sets of these images as $\mathcal{D}_b$ and $\mathcal{D}_a$, respectively.

2. For every recipient, we digitize a layer of polygons over every occluded road surface, and refer to the set of these areas as $O_r$.

3. For every donor $d$, and for every recipient $r$ that is in the same period $t = \{b, a\}$ as $d$, we partition $L_d$ into $\tilde{L}_d^r$, the set of vehicle locations that would be counterfactually occluded under the occlusion layer $O_r$, and $\tilde{L}_d^{-r}$, the set of vehicles that would remain visible under the counterfactual occlusion layer $O_r$.

4. For every recipient $r$ in period $t = \{b, a\}$, we assemble a donor pool of every observed but counterfactually occluded vehicle location $P_r = \bigcup_{d \in \mathcal{D}_t} \tilde{L}_d^r$.

5. We define the augmented vehicle location set $L_r^+ = L_r \cup P_r$, where to each element in $L_r$ we attach a weight of 1, and to each element in $P_r$ from donor $d$ we assign the scalar weight $w_{dr} = (1/(|\mathcal{D}_t|)) \left[ |L_r| / (|L_d| - |\tilde{L}_d^r|) \right]$.

The first factor in the weight $w_{dr}$ simply averages over the set of donors. The second maintains proportionality between vehicle counts in the image areas that are mutually observed in the recipient and each donor image. For example, if donor $d$ contains half as many vehicles as a recipient $r$ in the area that is mutually observable in both images, any vehicle locations donated from $d$ to $r$ will be weighted by $1/2$, and further re-weighted in proportion to the number of donor images. We apply the above procedure separately for each area of interest and vehicle type.

Buildings in area (i) are relatively low and imputations have little impact on counts and densities: although 16 of 29 images contain some imputations, imputations only increase the total vehicle count in this area by 1.1% and additions to the sample are only substantial in four images: the five largest percentage increases in weighted vehicle

count are 11.3%, 10.1%, 7.8%, 7.8% and 1.2%. Area (ii) in midtown Manhattan is dense with skyscrapers, so even small deviations from a perpendicular angle in aerial photography can result in road occlusion. The imputation procedure described above increases the total vehicle count by 6.1% in this area, with imputed vehicles added to 22 scenes. The vehicle count is increased by more than 10% in 8 scenes, and between 10 and 1% in a further 9 scenes. Details on raw, imputed and total counts for both areas are provided in Tables B.1 and B.2 below.

Table B.1: Aerial imagery sources and counts. Upper East Side and East Harlem

| Date | Source | Raw count | Imputed | Total | Time of day |
|---|---|---|---|---|---|
| 6/15/2010 | NYC Ortho | 2,819 | | 2,819.0 | 10:30 am |
| 6/17/2010 | Google Earth | 2,314 | 181.2 | 2,495.2 | 10:15 am |
| 3/26/2011 | ESRI Aerial | 1,649 | 2.5 | 1,651.5 | 12:30 pm |
| 6/2/2011 | Google Earth | 3,279 | | 3,279.0 | 11:45 am |
| 7/10/2011 | NAIP | 1,920 | 3.7 | 1,923.7 | 12:30 pm |
| 3/10/2012 | Google Earth | 1,708 | | 1,708.0 | 11:30 am |
| 6/15/2012 to 6/20/2012 | NYC Ortho | 3,271 | | 3,271.0 | 11:15 am |
| 8/6/2012 | Google Earth | 2,786 | | 2,786.0 | 9:30 am |
| 11/5/2012 | Google Earth | 2,423 | 274.4 | 2,697.4 | 10:30 am |
| 5/26/2013 | Google Earth | 1,257 | | 1,257.0 | 11:00 am |
| 6/22/2013 | NAIP | 1,297 | 100.6 | 1,397.6 | 8:30 am |
| 6/1/2014 | NYC Ortho | 2,160 | 27.1 | 2,187.1 | 11:00 am |
| 6/19/2014 | Google Earth | 3,120 | 11.8 | 3,131.8 | 12:30 pm |
| 7/6/2014 to 8/10/2014 | Bing Aerial | 2,657 | | 2,657.0 | 9:15 am |
| 9/15/2014 | Nearmap | 2,893 | | 2,893.0 | 9:40 am to 10:08 am |
| 10/11/2014 | Google Earth | 1,150 | 116.4 | 1,266.4 | 10:45 am |
| 4/12/2015 | Nearmap | 2,686 | 3.9 | 2,689.9 | 2:44 pm to 3:11 pm |
| 5/22/2015 | NAIP | 2,770 | 2.3 | 2,772.3 | 9:45 am |
| 6/22/2015 | Nearmap | 3,016 | | 3,016.0 | 10:15 am to 10:47 am |
| 9/6/2015 | Google Earth | 1,223 | 0.2 | 1,223.2 | 11:30 am |
| 9/6/2015 | Nearmap | 1,884 | | 1,884.0 | 1:01 pm to 1:30 pm |
| 10/26/2015 | Nearmap | 2,574 | | 2,574.0 | 11:35 am to 12:03 pm |
| 3/26/2016 to 4/5/2016 | NYC Ortho | 3,750 | | 3,750.0 | 12:45 pm |
| 4/16/2016 | Nearmap | 2,534 | 14.3 | 2,548.3 | 11:31 am to 12:09 pm |
| 6/24/2016 | Google Earth | 2,123 | 0.3 | 2,123.3 | 11:30 am |
| 6/25/2016 | Google Earth | 1,617 | 1.4 | 1,618.4 | 11:30 am |
| 7/16/2016 | Nearmap | 1,876 | | 1,876.0 | 11:11 am to 11:37 am |
| 10/15/2016 | Nearmap | 2,667 | 7.0 | 2,674.0 | 11:34 am to 11:58 am |
| 4/9/2017 | Nearmap | 2,632 | 3.8 | 2,635.8 | 1:05 pm to 1:27 pm |

Note: Capture dates are provided in metadata for all sources, except two NYC scenes for which a date range is provided, and the Bing Aerial layer which was captured between July 6 and August 10, 2014 according to imagery service API metadata. Time-of-day of image capture is provided in a precise range by Nearmap. For other sources, the time-of-day is estimated by using the shade of the Columbus Circle monument as a sundial (calendar-adjusted). Building shadows in area of interest are consistent with monument shadows. Nearmap metadata and imagery validates our sundial method to within half-hour accuracy.

Table B.2: Aerial imagery sources and counts. Midtown

| Date | Source | Raw count | Imputed | Total | Time of day |
|---|---|---|---|---|---|
| 6/15/2010 | NYC Ortho | 3,162 | | 3,162.0 | 10:30 am |
| 6/17/2010 | Google Earth | 1,815 | 463.8 | 2,278.8 | 10:15 am |
| 3/26/2011 | ESRI Aerial | 1,032 | 556.2 | 1,588.2 | 12:30 pm |
| 6/2/2011 | Google Earth | 2,886 | 17.3 | 2,903.3 | 11:45 am |
| 7/10/2011 | NAIP | 1,930 | | 1,930.0 | 12:30 pm |
| 3/10/2012 | Google Earth | 1,589 | 7.4 | 1,596.4 | 11:30 am |
| 6/15/2012 to 6/20/2012 | NYC Ortho | 3,590 | | 3,590.0 | 11:15 am |
| 8/6/2012 | Google Earth | 3,150 | 65.6 | 3,215.6 | 9:30 am |
| 11/5/2012 | Google Earth | 1,430 | 701.2 | 2,131.2 | 10:30 am |
| 5/26/2013 | Google Earth | 1,110 | 10.9 | 1,120.9 | 11:00 am |
| 6/22/2013 | NAIP | 828 | 296.1 | 1,124.1 | 8:30 am |
| 6/1/2014 | NYC Ortho | 1,929 | 194.0 | 2,123.0 | 11:00 am |
| 6/19/2014 | Google Earth | 2,497 | 21.2 | 2,518.2 | 12:30 pm |
| 7/6/2014 to 8/10/2014 | Bing Aerial | 2,167 | | 2,167.0 | 9:15 am |
| 9/15/2014 | Nearmap | 3,557 | | 3,557.0 | 8:34 am to 10:09 am |
| 10/11/2014 | Google Earth | 1,017 | 222.1 | 1,239.1 | 10:45 am |
| 4/12/2015 | Nearmap | 2,361 | 55.3 | 2,411.3 | 3:11 pm to 3:30 pm |
| 5/22/2015 | NAIP | 2,817 | 303.3 | 3,120.3 | 9:45 am |
| 6/22/2015 | Nearmap | 3,137 | | 3,137.0 | 10:10 am to 10:38 am |
| 9/6/2015 | Google Earth | 987 | 14.3 | 1,001.3 | 11:30 am |
| 9/6/2015 | Nearmap | 1,989 | 174.9 | 2,163.9 | 12:43 pm to 1:01 pm |
| 10/26/2015 | Nearmap | 2,229 | 94.8 | 2,323.8 | 11:15 am to 11:34 am |
| 3/26/2016 to 4/5/2016 | NYC Ortho | 3,867 | | 3,867.0 | 12:45 pm |
| 4/16/2016 | Nearmap | 1,965 | 114.8 | 2,079.8 | 12:00 to 12:18 pm |
| 6/24/2016 | Google Earth | 2,270 | 109.9 | 2,379.9 | 11:30 am |
| 6/25/2016 | Google Earth | 2,132 | 221.6 | 2,353.6 | 11:30 am |
| 7/16/2016 | Nearmap | 1,879 | 50.5 | 1,929.5 | 11:04 am to 11:36 am |
| 10/15/2016 | Nearmap | 2,437 | 111.1 | 2,548.1 | 11:18 am to 11:26 am |
| 4/9/2017 | Nearmap | 2,107 | 82.5 | 2,189.5 | 12:56 pm to 1:04 pm |

# Appendix C  Evidence of the slowdown in New York City streets and highways



(a) Medians, 342 pairs between 19 midtown zones

(b) 10th perc., 72 pairs to 4 zones on East River

(c) 90th perc., 72 pairs to 4 zones on East River

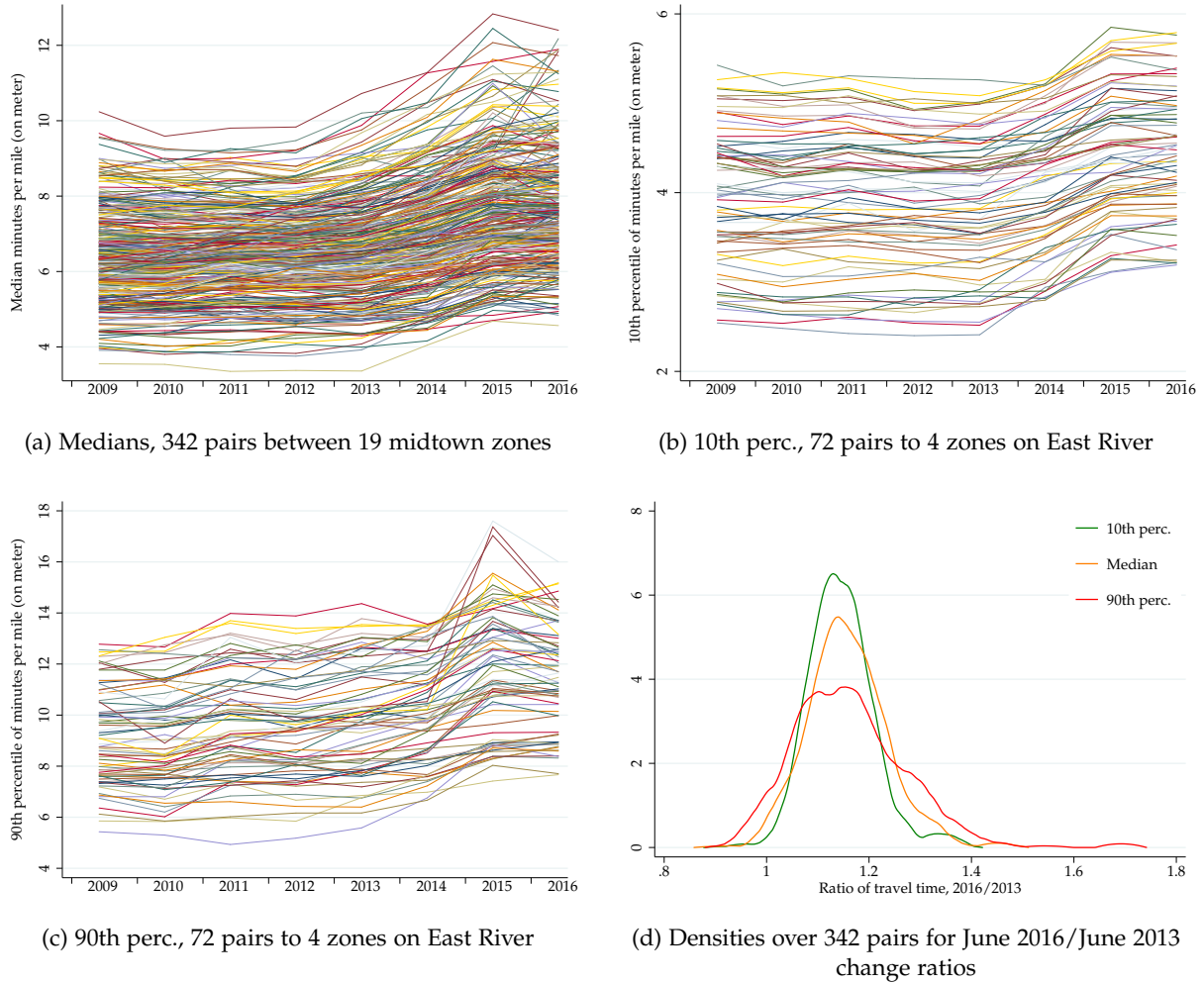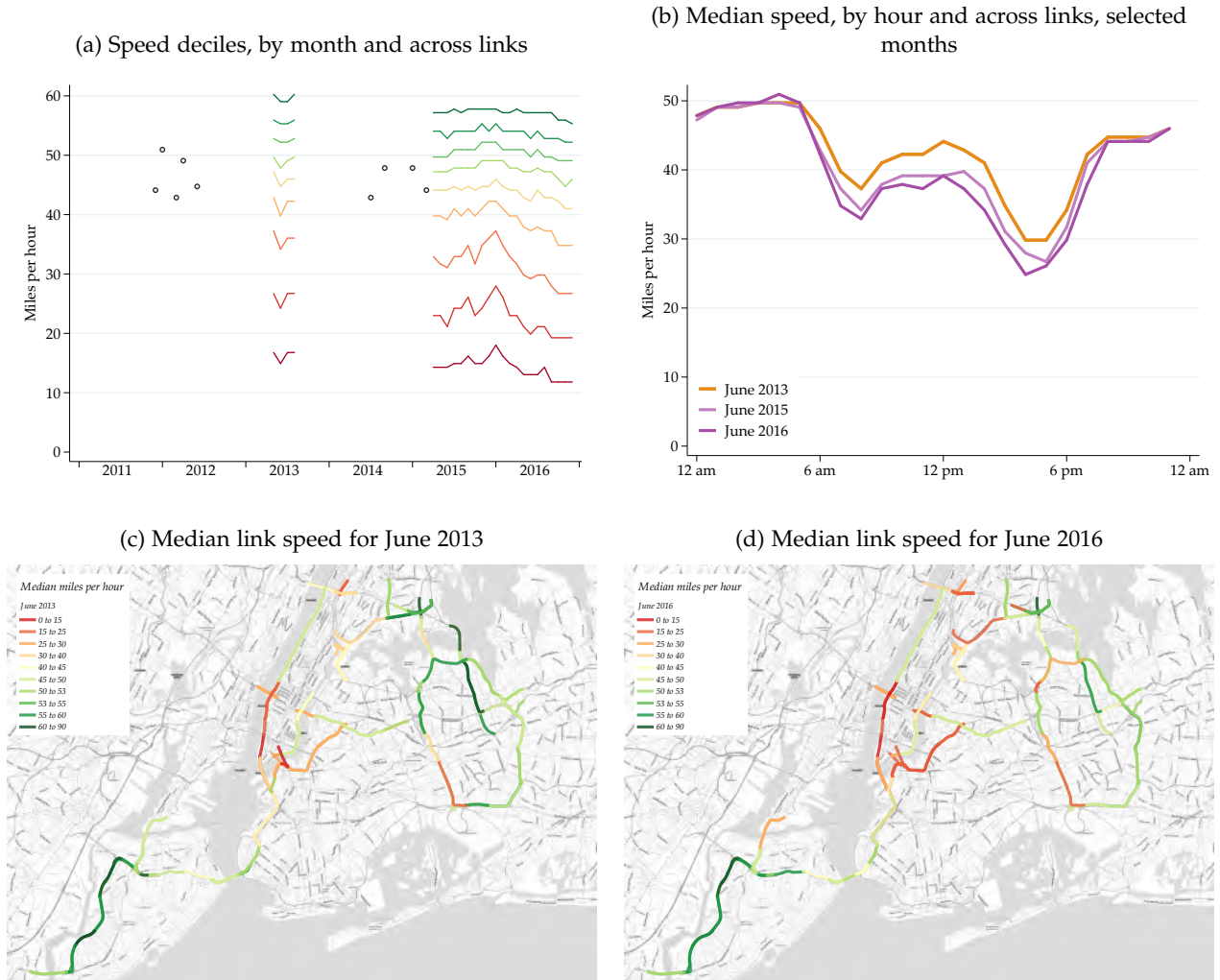(d) Densities over 342 pairs for June 2016/June 2013 change ratios

Figure C.2: Travel times (percentiles of minutes per mile) for origin-destination pairs in midtown Manhattan, month of June 2009 to 2016

Note: All figures are constructed from raw coordinates on TPEP trip data matched to "taxi zones," during the month of June from 2009 to 2016. The measures plotted are quantiles of the minutes per mile on the taxi meter. "Taxi zones" are a neighborhood-level unit of spatial aggregation defined by the TLC and at which for-hire-vehicle bases (e.g. livery, ridehail) are required to report trip originations. Midtown Manhattan between 14th and 59th streets contains 19 taxi zones. Densities in Figure C.2d are weighted by trips in June 2013.

## Figure C.3: Historical speeds, archived from live EZ-Pass traffic sensor feeds

(a) Speed deciles, by month and across links



(b) Median speed, by hour and across links, selected months



(c) Median link speed for June 2013



(d) Median link speed for June 2016



Note: Speeds are obtained from archived feeds of live sensor data from the NY State EZ-Pass traffic monitoring system. Sources are described in Appendix A. Fig. (a) plots the time series for deciles of all EZ-pass traffic sensor speed measurements (10th to 90th percentile, in miles per hour) and across all links in a given month (subselections of this data, such as weekdays during daytime, display similar patterns). Percentiles are plotted as lines from May 2013 through August 2013 and from April 2015 onwards, which are the months for which continuously archived data is available. Black circles plot the median speed across links for single snapshots of the data that were archived by archive.org, for nine additional months in which some of this data is available. Fig. (b) plots median speeds across links per hour for the month of June in 2013, 2015 and 2016. Figures (c) and (d) map the median speeds at the link level for June 2013 and June 2016, respectively. On both maps the speed levels are displayed on a color ramp that corresponds approximately to deciles of the speed distribution in June 2013, as plotted in the time series shown in fig. (a). The network of road segments linked through EZ-pass sensors has extended over time, the maps in figures (c) and (d) plot the 115 segments that were active in June 2013 and June 2016. Links contain overalapping segments, which are shown by means of transparencies.

63

Note: methodology is described in Appendix E. In particular, note that plotted bounds arise from limiting methodological assumptions, and are not confidence intervals. Figure (a) plots the daily average of interpolated miles per day per VIN for each class of vehicles, with orange for taxis, green for boro taxis and purple for all for-hire vehicles. Miles per day per VIN require two odometer inspections around the interpolation date. Figures (b)-(c) plot the estimated stock of registered vehicles per day, and figures (d)-(e) plot an estimate of vehicle-miles traveled per day, i.e. the product of the vehicle stock times the daily average flow of miles per day per VIN for each class. In figures (b) and (d) the color yellow indicates yellow taxis, whereas green indicates yellow plus boro taxis.
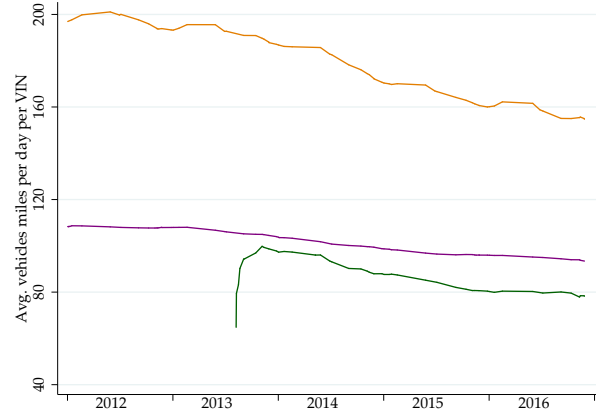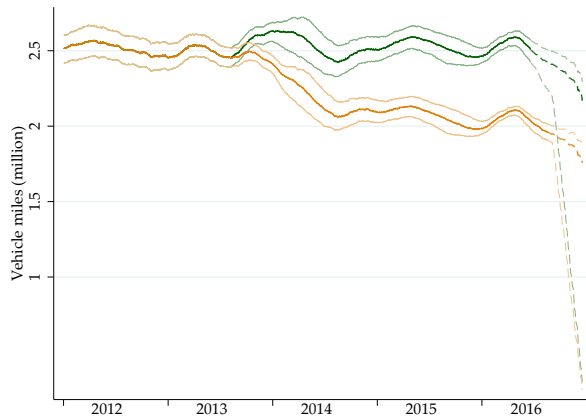
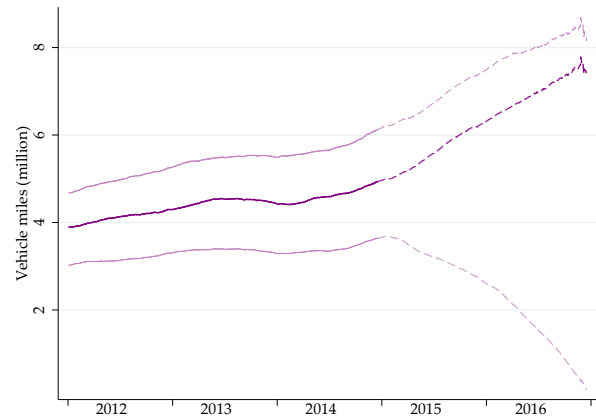(a) Avg. miles per day per VIN and class interpolated from odometer readings
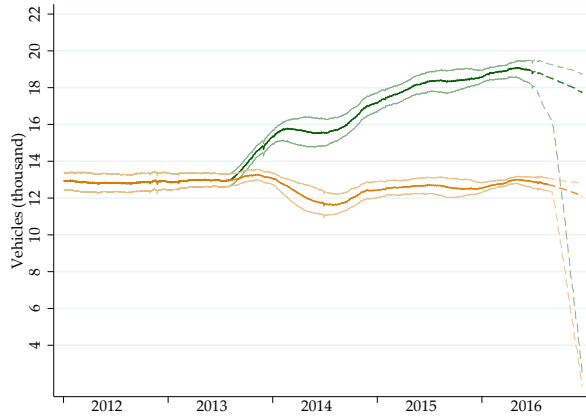
(b) Stock of registered yellow and boro taxis
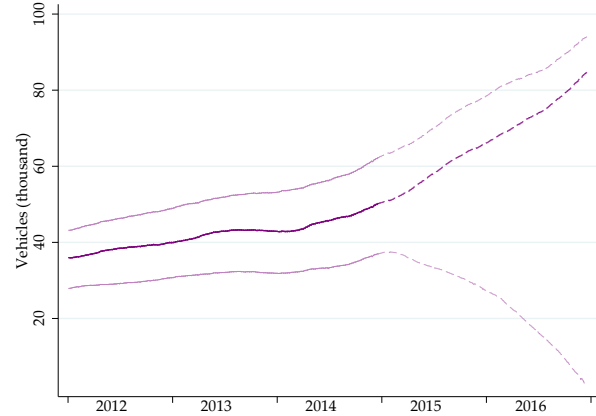
(c) Stock of registered for-hire vehicles

(d) Yellow and boro taxi total VMTs per day

(e) For-hire vehicle total VMTs per day

Figure C.4: Vehicle miles traveled (VMTs) by vehicle class, estimated from odometer data

# Appendix D    GPS data validation (For online publication)

This paper employs geographic coordinates of taxi pickups and drop-offs recorded by GPS units onboard taxis (TPEP units) to construct historical speed measures and to track the location of taxi activity. In this appendix, we evaluate the robustness of our identification strategy (in particular, our reduced form estimates) to measurement error in these geographic coordinates. Although there is no obvious direction of bias, GPS accuracy in our area and period of study was subject to spatial and time trends that could, in principle, act as a confounder.

The accuracy of navigation satellite systems depends on the number of signal-emitting satellites within line-of-sight of the receiver, and tall buildings may create "urban canyons" that reduce the number of satellites in view. In northern Manhattan the height and density of buildings increases in the downtown direction. Since the height of buildings surrounding a road segment rarely changes, GPS accuracy could be a time-invariant attribute of road segments that can be controlled for with road segment fixed effects (i.e. run-bin f.e. in the notation used in the paper). However, the number of "GPS satellites" that at any given moment are directly overhead and available to receivers in New York City has increased substantially in the past decade with the deployment of satellite systems from Russia, the European Union and China.[51] If trends in GPS satellite availability have a differential impact on coordinate accuracy that depends on the heights of surrounding buildings, GPS accuracy could follow differential trends across the boro and "hail-exclusion" zones.

We employ two measures of potential satellite obstruction throughout northern Manhattan, illustrated in Figure D.5: the average number of floors of the buildings that overlap a road segment in the area of interest (floor numbers are color-coded in blue), and a measurement of sky-view factor (SVF), which is the share of sky in a hemispherical field of vision from the ground. We employ SVF measures from Liang *et al.* (2017), which were computed from Google Street View imagery at the midpoint of every city block in Manhattan. Figure D.5 illustrates that building height (and sky-view-factor) are correlated with latitude in northern Manhattan.[52] Table D.3 estimates the baseline reduced form result from Table 5, Col. 2 while including controls for trends in GPS accuracy. Col. 1 includes the average number of completed floors for the buildings with a footprint that overlaps each 10 meter segment (i.e. bin) on every avenue. This control has no impact on the coefficient of interest, which is not surprising since it contains almost no variation over time and all of its cross-sectional variation was previously absorbed by run-bin fixed effects. Col 2. interacts quartiles of the previous measure with linear trends, to allow for arbitrary differential linear trends over ranges of building heights. Col. 3 interacts linear trends with quartiles of street-

---

[51] GPS is a name that is specific to the United States government's global navigation satellite system, which was fully deployed to its current constellation size (32 satellites) and coverage level prior to 2009. The satellite constellations of Russia (GLONASS), the EU (Galileo) and China (BeiDou2) have been expanded between January 2009 and June 2016, with net gains of 7, 9 and 19 satellites respectively. The satellites of these systems emit signals that are available to consumer "GPS" units, and the expansion has allowed for significant accuracy improvements worldwide.

[52] Park Avenue is an exception, as it is separated by elevated tracks north of East 101st Street.

view-factors, where values for bins in which Liang *et al.* (2017) did not calculate a factor are interpolated from neighboring measures: the estimated coefficient barely changes. Results from Cols. 2 and 3 suggest that any differential trends in GPS accuracy by level of urban density did not have an impact on the measurement of street-speed that correlates in space and time with the roll-out of the boro program.

We next employ a direct measure of taxi GPS accuracy: we filter all the taxi pickup or drop-off coordinates in our area of interest through the building footprints in the area. Although coordinates may be in error even if recorded at a street curb, one type of error that we can measure over space and time is the share of trip endpoints that were placed by the taxi's GPS unit within the walls of an existing structure. Using this definition of GPS accuracy we do find that accuracy evolved differently over the treatment and control zones: 8.8% of trip endpoints in the hail-exclusion zone, and 5.4% in the boro zone were located within a building footprint in the 56 months leading up to August 2013, whereas fail rates declined to 7.2% and 2.6%, respectively, in the 34 months from September 2013 onward. Apparently, the deployment of additional satellites has had a larger effect on the accuracy of GPS fixes at an intermediate rather than at the higher end of urban density. Columns 4 and 5 include levels and logs of this GPS failure rate. Once again, our baseline estimate of the impact of the boro program is not sensitive to the inclusion of this control for GPS accuracy.
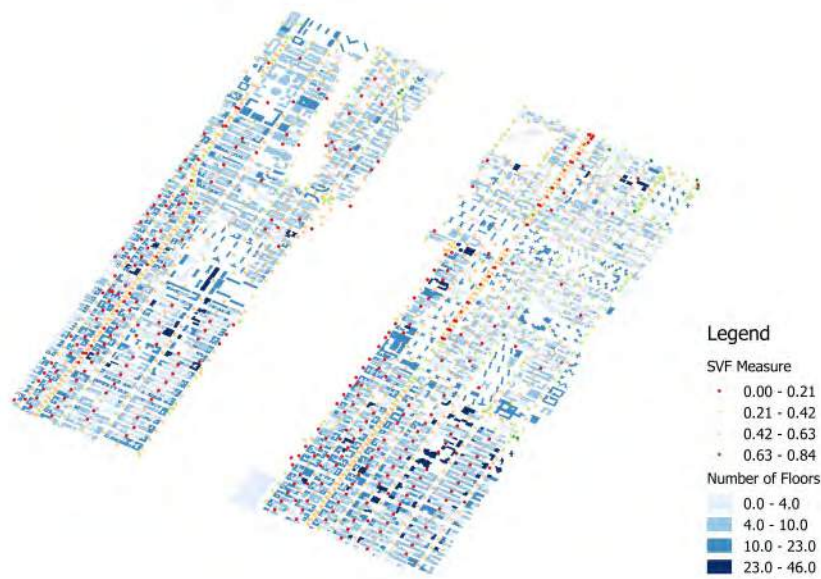


Figure D.5: Building footprints, number of floors and sky-view factors

Note: Sky-view factor (SVF) is the share of the vertical field of vision that is composed of sky. SVF measures were computed by Liang *et al.* (2017) from Google Street View imagery. Building footprints and number of floors are from data.cityofnewyork.us/Housing-Development/Building-Footprints/nqwf-w8eh.

Table D.3: Robustness of reduced form impact to measurement error in GPS units

| | (1) | (2) | (3) | (4) | (5) |
|---|---|---|---|---|---|
| | Log avg. s/m | Log avg. s/m | Log avg. s/m | Log avg. s/m | Log avg. s/m |
| BZ x Roll-out | 0.081 | 0.081 | 0.078 | 0.081 | 0.081 |
| | (0.004) | (0.004) | (0.004) | (0.004) | (0.004) |
| | | | | | |
| Avg. number of floors | 0.000 | | | | |
| | (0.000) | | | | |
| | | | | | |
| Avg. num. floors: quartiles × linear trends | | Y | | | |
| | | | | | |
| Sky view factor: quartiles × linear trends | | | Y | | |
| | | | | | |
| GPS fail rate | | | | 0.008 | |
| | | | | (0.002) | |
| | | | | | |
| Log GPS fail rate | | | | | 0.000 |
| | | | | | (0.000) |
| Standard controls | Y | Y | Y | Y | Y |
| Run-bin × Run-my FE | Y | Y | Y | Y | Y |
| Observations | 406260 | 406260 | 402750 | 406260 | 406260 |
| $R^2$ | 0.97 | 0.97 | 0.97 | 0.97 | 0.97 |
| $R^2$-within | 0.15 | 0.15 | 0.15 | 0.15 | 0.15 |

Note: Unless otherwise specified, robust standard errors are two-way clustered at the level of run× bin and run× month. In Col. 3, street-view-factors are interpolated from neighboring measures for bins without data from Liang *et al.* (2017), and 39 bins are dropped from the sample due to lack of data for interpolation. The estimated coefficient on the subsample of 1,098 bins for which SVFs are available is almost unchanged. Cols. 2 and 3 include interactions of GPS accuracy determinants with linear trends; interactions with the *post* dummy or the *Boro roll-out* trend also have no effect on the coefficient of interest.

# Appendix E    Method for estimating vehicle miles traveled from odometer inspection data (For online publication)

In this appendix we explain our methodology for calculating the total number of vehicle-miles traveled (VMTs) per day for each of the following classes of vehicles: yellow taxis, boro taxis and for-hire vehicles (FHVs), the latter a class that includes traditional black cars and other car services as well as, more recently, ridehail providers. We employ odometer readings per vehicle identification number (VIN) from 2010 through 2016, measured at regular inspections required by the Vehicle Inspection Program of New York City's Taxi and Limousine Commission and obtained through freedom-of-information requests.

Vehicles in each class are required to undergo regular inspections: within 3 months for yellow taxis, 6 months for boro taxis and 2 years for FHVs. The empirical challenge to estimating time series of VMTs from regular odometer inspections is that the data is naturally censored. Vehicles require an inspection to enter car service, but may exit car service at any point after an inspection, and this exit will not be observed until the vehicle fails to show up for an inspection within the required window. To address this missing data problem, we separately estimate daily flows of VMTs from the daily stock of vehicles on the road. Estimating average mile flows conditional on the set of vehicles that are confirmed survivors (i.e. are between inspections) is straightforward: we interpolate the odometer readings for each survivor to obtain daily flows, and average these daily flows over all survivors.

Accounting for censoring is more involved. We cannot estimate the timing of exit because we do not observe exit dates on any part of our sample; we only observe whether vehicles fail to show within the re-inspection window. Additionally, censoring interacts with the end date of our inspection sample (December 31, 2016) to create a period of uncertain exit. We use FHVs as an example hereafter but employ the same approach for each class of vehicles: whereas we can be certain that a VIN that was last seen prior to December 31, 2014 has exited FHV service some time over the following two years, any VIN that was last observed from January 1, 2015 onwards may have exited or may still be in service as of December 31, 2016.

Using the subsample of VIN-inspection dates for which a subsequent re-inspection or exit has occurred with certainty, we estimate the 2-year survival rate for each interval of 50,000 miles on the odometer (through 400K miles, all higher mileages are binned together). We then compute the stock of vehicles on the road as of date $t$ as the sum of confirmed survivors (i.e. the VIN is re-inspected after $t$) plus an estimate of expected survivors, which consist of expected confirmed exiters (since exit date is not identified, we assume it is equiprobable over the inspection window) and expected uncertain exiters (we assume the constant hazard rate that accumulates to the estimated 2-year survival rate). We then compute our baseline daily VMT estimates as the product of daily average VMT flows per VIN and the expected stock of active VINs.

Out of necessity, our approach makes two strong assumptions: equiprobable daily exit rates for confirmed exiters and constant hazard rates for uncertain exiters. As bounds on the previous approach, we consider two alternative assumptions: we obtain

an upper bound by assuming that all vehicles survive until we observe them to miss a re-inspection date, and a lower bound by assuming exit immediately after the last inspection. Note that the lower bound approach mechanically drives down the stock of estimated cars during the uncertain exit window, all the way down to zero on Jan 1, 2017.

Our estimate of daily VMT flows per vehicle, as well as baseline and bound estimates for stocks and total VMT flows are plotted in Figure C.4. Note that shorter re-inspection windows for yellow taxis result in tighter estimates and shorter uncertain exit periods. We start our plots on January 1, 2012 since a symmetric source of uncertainty over entry occurs at the start of our sample period. We do not allocate FHVs miles between ridehail and traditional car services. We do not believe that this is possible without de-anonymized, VIN level data from ridehail providers because vehicles affiliated to traditional car service bases are supplied on ridehail platforms. Throughout our application we employ the sum of both modes as the unit of analysis.

# Appendix F  Additional figures and tables
## (For online publication)

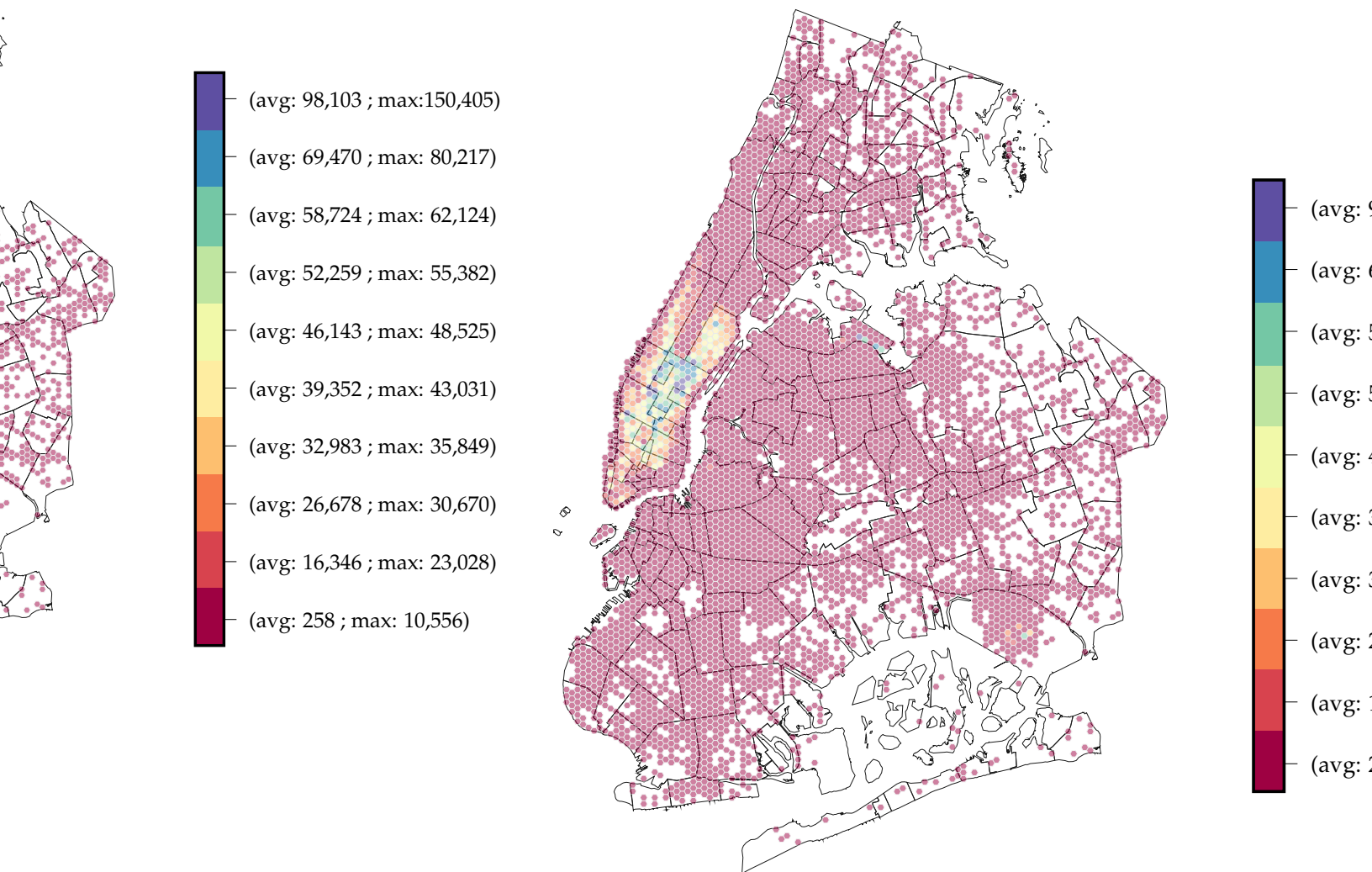Table F.4: Wald estimates of the congestion elasticity of taxi pickups. Spline speeds

| | (1) | (2) | (3) | (4) | (5) | (6) |
|---|---|---|---|---|---|---|
| | Log Bsp. s/m | Log Bsp. s/m | Log Bsp. s/m | Log Bsp. s/m | Log Bsp. s/m | Log Bsp. s/m |
| | (OLS) | (2SLS) | (OLS) | (2SLS) | (OLS) | (2SLS) |
| Log pickups | -0.006 | 0.132 | -0.005 | 0.188 | 0.002 | 0.038 |
| | (0.006) | (0.027) | (0.007) | (0.038) | (0.007) | (0.023) |
| Bikelane | -0.071 | -0.106 | -0.183 | -0.271 | 0.122 | 0.125 |
| | (0.052) | (0.056) | (0.077) | (0.087) | (0.041) | (0.041) |
| Citibike | 0.062 | 0.115 | 0.080 | 0.156 | 0.036 | 0.049 |
| | (0.035) | (0.039) | (0.049) | (0.055) | (0.016) | (0.020) |
| 311 complaints | 0.003 | 0.002 | 0.004 | 0.003 | 0.001 | 0.001 |
| | (0.003) | (0.003) | (0.005) | (0.005) | (0.002) | (0.002) |
| Potholes | -0.005 | -0.007 | -0.033 | -0.037 | 0.023 | 0.023 |
| | (0.009) | (0.010) | (0.017) | (0.018) | (0.007) | (0.007) |
| Run-bin and Run-m-y FE | Y | Y | Y | Y | Y | Y |
| Sample | All | All | East side | East side | West side | West side |
| Observations | 406260 | 406260 | 216000 | 216000 | 190260 | 190260 |
| $R^2$ | 0.64 | 0.63 | 0.54 | 0.53 | 0.74 | 0.74 |

Note: Unless otherwise specified, robust standard errors are two-way clustered at the level of run$\times$ bin and run$\times$ month. Weak instrument tests are not reported, but the lowest F-stat in the table (for column 9, the West side, Bspline specification) is 35,315. About 1.16% of the 10-meter avenue segments had no taxi pickups within a particular month: we set the dependent variable at $log(\text{pickups} + 0.1)$.

Table F.5: Program impact coefficient by time slice

|  | 24 hrs. | 6am-8pm | 6am-10am | 10am-2pm | 2pm-4pm | 4pm-8pm | 8pm-11pm | 11pm-6am |
|---|---|---|---|---|---|---|---|---|
| Full week coef. | 0.081 | 0.080 | 0.067 | 0.091 | 0.052 | 0.094 | 0.079 | 0.080 |
| Std. err. | (0.004) | (0.004) | (0.006) | (0.006) | (0.006) | (0.005) | (0.005) | (0.007) |
| Avg. trips per run-month-bin | 1824.4 | 1391.4 | 286.2 | 398.2 | 230.1 | 477.0 | 236.4 | 196.6 |
| Weekday coef. | 0.077 | 0.074 | 0.061 | 0.081 | 0.043 | 0.097 | 0.076 | 0.065 |
| Std. err. | (0.005) | (0.005) | (0.007) | (0.006) | (0.007) | (0.005) | (0.006) | (0.007) |
| Avg. trips per run-month-bin | 1306.3 | 1019.5 | 225.8 | 268.8 | 167.9 | 357.0 | 171.0 | 133.5 |
| Weekend coef. | 0.071 | 0.068 | 0.045 | 0.072 | 0.061 | 0.073 | 0.091 | 0.104 |
| Std. err. | (0.005) | (0.005) | (0.007) | (0.006) | (0.008) | (0.007) | (0.008) | (0.008) |
| Avg. trips per run-month-bin | 518.2 | 371.9 | 60.4 | 129.3 | 62.2 | 120.1 | 65.4 | 120.0 |

Note: This table reports variations on the the baseline program impact regression (i.e. Column 2 of Table 6) in which the average second-per-meter outcome measure is computed under alternative time slices of the within-run trip data sample. The table is ordered in rows for day-of-week and columns for time-of-day slices, and the top left cell is the same specification as Table 6, Col. 2. Each cell reports estimated coefficient and standard errors for the boro-zone times roll-out interaction, as well as the average number of trips used in computation of the average travel time for each run, month and 10 meter bin.

(avg: 98,103 ; max:150,405)

(avg: 69,470 ; max: 80,217)

(avg: 58,724 ; max: 62,124)

(avg: 52,259 ; max: 55,382)

(avg: 46,143 ; max: 48,525)

(avg: 39,352 ; max: 43,031)

(avg: 32,983 ; max: 35,849)

(avg: 26,678 ; max: 30,670)

(avg: 16,346 ; max: 23,028)

(avg: 258 ; max: 10,556)

Note: Raw taxi records (TPEP data, described in Appendix A) for all pickups within New York City during June 2013, binned into 12,004 hexagonal cells (each with an area of 0.081 sq. km, or 19.8 acres). Every color shade accounts for approximately one tenth (1.4 million) of all taxi pickups. For example, the 14 hexagonal cells in purple accounted for 9.73% of all pickups in June 2013, with an average 98,103 pickups per cell, a volume of pickups that is equal to that of the area shaded in red (average 258 pickups per cell) and white (no pickups). Numbers on the color bar indicate the average and maximum number of pickups over the cells in a given color.

Figure F.7: Traffic speeds and taxi pickups
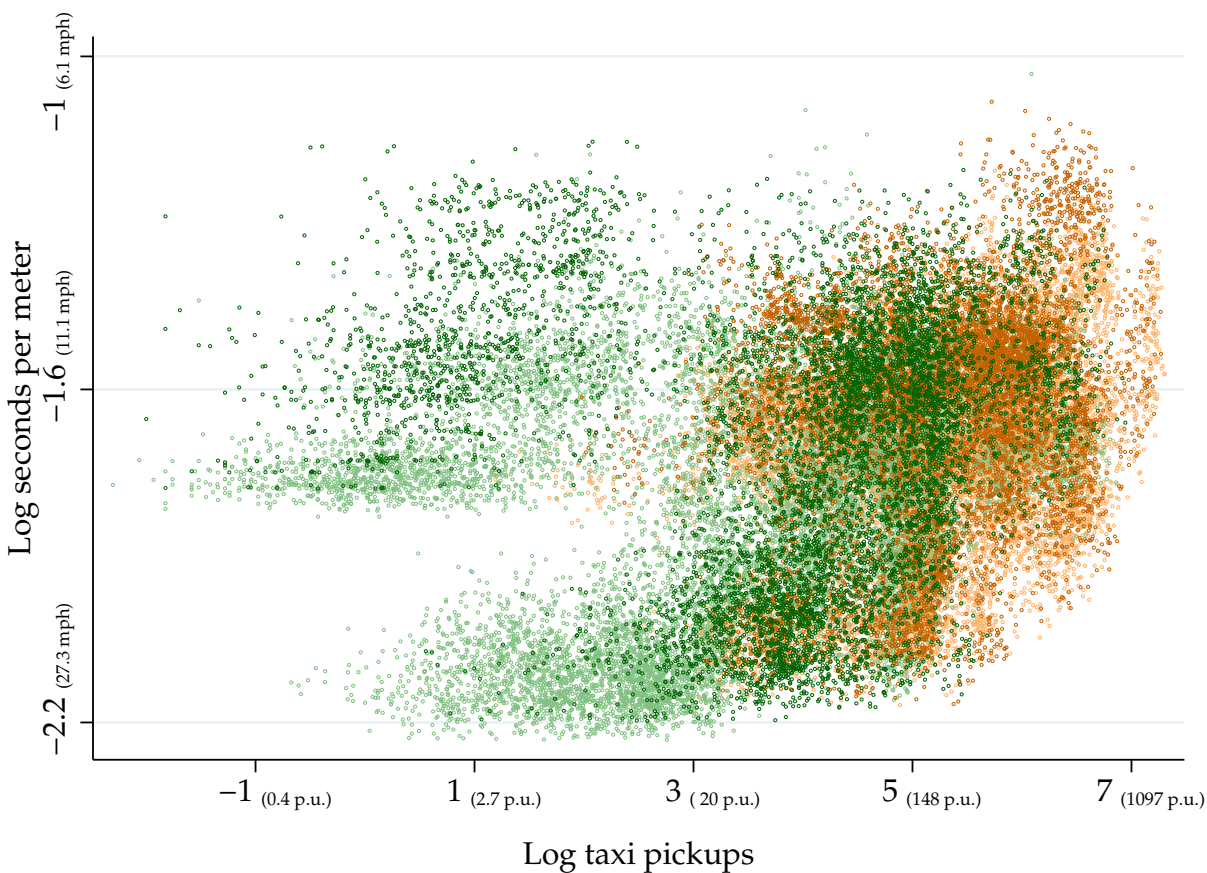


Note: Sample from Table 9, Cols. 1-3. Treatment status and period is indicated by color and shade, according to the following scheme: bins in the treatment "boro" zone are green, control are orange; pre period in a light shade and post period in a dark shade. Each point is the average for both variables of 10 contiguous bins on a given run and month. Axes are in log travel time and log pickups, but absolute values for speed and pickups are included for convenience.